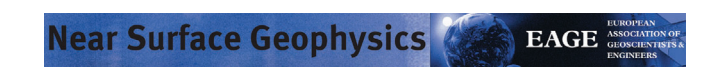
#### **ORIGINAL ARTICLE**



# Influence of subsurface refraction and wave travel path on the estimation of average $V_S$ profiles from the seismic downhole test

#### Ayush Kumar | Anbazhagan Panjamani

Department of Civil Engineering, Indian Institute of Science, Bangalore, India

#### Correspondence

Anbazhagan Panjamani, Department of Civil Engineering, Indian Institute of Science, Bangalore, India.

Email: anbazhagan@iisc.ac.in

#### **Funding information**

Capacity Buildings in Dam Safety; Dam Safety (Rehabilitation) Directorate, Central Water Commission, Govt. of India; Dam Rehabilitation and Improvement Project; SERB, DST, Govt. of India; Liquefaction Potential Assessment, Grant/Award Number: SERB/F/198/2017-18; M/s Secon Pvt. Ltd., Grant/Award Number: SP/SECO-18-0001; Effect of shear wave velocity calibration on Amplification of shallow and deep soil sites, Grant/Award Number: SECON/IISc/MoES/WO/07-18/0079

#### **Abstract**

The Downhole (DH) seismic test is an important geophysical exploration method and has become an essential tool for determining subsurface dynamic properties and seismic site class. To analyse the acquired data, an approximation of a straight raypath is often assumed between the source and receiver, which neglects refractions along the travel path due to changes in subsurface properties. Further investigation is needed to fully understand the effects of subsurface refraction on the determination of total travel length and average S-wave velocity  $(V_S)$ . Hence, DH tests at several locations up to a depth of over 30 m were conducted in this study. Average  $V_S$  profiles were determined considering a straight travel path and refraction occurring along the travel path. It was observed that the average V<sub>S</sub> values remain fairly independent of the inversion method used. The total refracted raypath length up to 30 m depth also shows no significant difference compared to a straight raypath. Similar observations were noted when the average  $V_S$  and raypath length from surface up to sediment depth and bedrock depth was calculated. Further, the ambiguity associated with the selection of a model for DH data reduction was studied, and minimal change was observed in average  $V_S$  with a change in depth of different subsurface interfaces. This observation concludes that the travel time from the source up to the 30 m depth and bedrock depth are sufficient for site classification if a detailed profile is not needed immediately. Further, the average  $V_S$  values obtained from DH tests were compared with commonly used MASW tests. The difference in average  $V_S$ up to bedrock and sediment depth from MASW and from DH test, considering both refracted raypath and straight raypath, was observed to be high for shallow bedrock sites. To study the effect of error in arrival time picking on average  $V_S$ profiles, random error within ±0.50 ms was introduced in arrival time data and  $V_{\rm S}$  profiles were estimated.

#### **KEYWORDS**

data processing, refraction, site characterization, S-wave, traveltime

#### INTRODUCTION

The impact assessment of earthquake shaking on structures requires the small-strain stiffness profile of the subsurface geological materials. These profiles depict variations in compression-wave (P) and shear-wave (S) velocities ( $V_p$  and  $V_S$ ) with depth and are determined in the field through seismic survey methods. Tradition-

ally, intrusive seismic techniques involving one or more boreholes have been employed, with the downhole (DH) method being the predominant choice over the last few decades (Bautista & Aguilar, 2023; Boore & Thompson, 2007; Butcher et al., 2005; Howard et al., 2008; Kim et al., 2004; Wang et al., 2021a, 2021b). The test is easy to perform with only one borehole and a simple seismic source arrangement consisting of a wooden beam and

a sledgehammer. In recent times, more extensive investigations have become necessary, especially at critical infrastructure sites like dams, nuclear power plants and industrial units. For projects of high importance, such as nuclear power plants, petrochemical investigations and deep investigations of fault systems, deep DH tests have also been conducted in the past two decades (Kumar & Anbazhagan, 2023; Stokoe et al., 2008, 2017; Vergniault & Mari, 2020). The improvement in DH test procedures and interpretation methods has also led to the use of seismic cone penetration tests for subsurface profiling and site classification purposes (Butcher et al., 2005; Campanella & Stewart, 1992; Vergniault & Mari, 2020; Wang et al., 2021b, 2022).

The DH test has recently gained importance with increasing microzonation and site amplification studies (Boore & Thompson, 2007; Borcherdt, 1994; Crice, 2011; Kim et al., 2004; Kumar & Anbazhagan, 2025). The test results are commonly used for the determination of average shear wave velocity up to 30 m  $(V_S^{30})$ , which is further used to determine seismic site class, or up to sediment depth or bedrock depth, which are also often used for site amplification studies (Bajaj & Anbazhagan, 2023; Boore & Thompson, 2007; Boore et al., 2021; Borcherdt, 1994). For estimation of  $V_S^{30}$ , or average  $V_S$  up to bedrock depth  $(V_S^{BR})$ , or average  $V_S$  up to soil thickness  $(V_S^{ST})$ , the average travel time from the concerned depth to the surface is considered, where  $V_{\rm S}$  and thickness of each layer are input parameters. The thickness of layers is calculated from the interface depths. Based on the depth-arrival time plot, there can be multiple interface depths possible depending upon the interpretation. The borelogs can assist in selection of depth of interfaces between different subsurface strata. Often, the interfaces detected from borelogs may not represent change in stiffness as expected (Bang et al., 2014; Boore & Thompson, 2007; Wang et al., 2021a). In such cases, the selection of interfaces needs to be done using arrival time-depth plot from DH data. However, instead of calculating the average travel time through each layer and adding them, the average  $V_{\rm S}$  can be calculated using the total travel time from surface to the acquisition depth, which is already known from DH test. Earlier, efforts have been made to improve the processing of DH data by considering the correct length of the travel path with refraction from source to the receiver (Bang et al., 2014; Boore & Thompson, 2007; Hallal & Cox, 2019; Kim et al., 2004). These studies did not discuss the influence of the refraction and the correction in the wave travel length on the average  $V_{\rm S}$  estimation. Earlier, Areias and Van Impe (2006) studied the effect of soil layers on rays travel path geometry using six simulated SCPT test cases without considering soil heterogeneity such as changes in  $V_{\rm S}$  with depth due to change in density and stress conditions. The deviation in raypath for increasing profile was observed to be 1.3%, which is

minimal, but for velocity inversion cases, the deviation in raypath calculation was higher at 4%. The maximum deviation was observed at the first interface and reduced with depth. The in situ conditions are always a mix of increasing and decreasing  $V_{\rm S}$  profiles, which warrant a more comprehensive study to look into the influence of such fluctuations in  $V_S$  profiles on raypath lengths and average  $V_{\rm S}$  profiles in detail. Hence, in this study an attempt has been made to demonstrate that  ${V_{\rm S}}^{30}$  or  ${V_{\rm S}}^{\rm BR}$  can be calculated with fair accuracy without determining the detailed  $V_S$  profile from the DH test. This outcome can save time and cost as the results can be obtained quickly.

#### **DOWNHOLE AND MASW TESTS**

The DH test is a simple, economical, faster procedure compared to the more detailed crosshole test and provides better resolution than the surface wavebased methods. The test is economical because a single borehole is required, which can also be utilized for subsurface sample collection for lab studies. Moreover, this test can help to get an average  $V_S$  and  $V_D$  at the required level from the surface, which is highly required for geotechnical design (ASTM D7400-2019; Boore & Thompson, 2007; Kumar & Anbazhagan, 2025). The standard procedure of the test follows ASTM D7400-2019. The test utilizes an impact-based or vibratory source placed on the ground surface to generate Pand S-waves. A static load is placed on the source to ensure firm contact between the source and the ground. A vertical impact is used to generate P-waves, and horizontal impact or oscillations are used to generate horizontally polarized shear (SH) waves. In this study, the impact-based source includes a 2 m long horizontal wooden plank with steel end caps upon which a vertical static load is placed and a sledgehammer. A geophone receiver or an array of geophones is installed vertically with depth in the borehole and moved further after each record. The receivers consist of 3-axis geophones with appropriate frequency and sensitivity characteristics, ensuring the accurate capture of the generated seismic wave (D7400-19, 2019; Kalinski, 2012). Figure 1 presents a schematic of the seismic DH test.

For accurate determination of the arrival of S-waves, the concept of polarity reversal is used (Campanella & Stewart, 1992; Kim & Park, 2002; Michaels, 2001). It is considered that the particle motion during the Swave traverse follows the excitation polarity, and the direction of motion reverses if the excitation direction is reversed. Figure 2 shows such records at different depths, acquired at horizontal channels normal to wave travel direction. This observation is also accompanied by a decrease in frequency and an increase in amplitude. Digital filters such as low pass, high pass and bandpass

FIGURE 1 A typical section schematic of seismic downhole test.

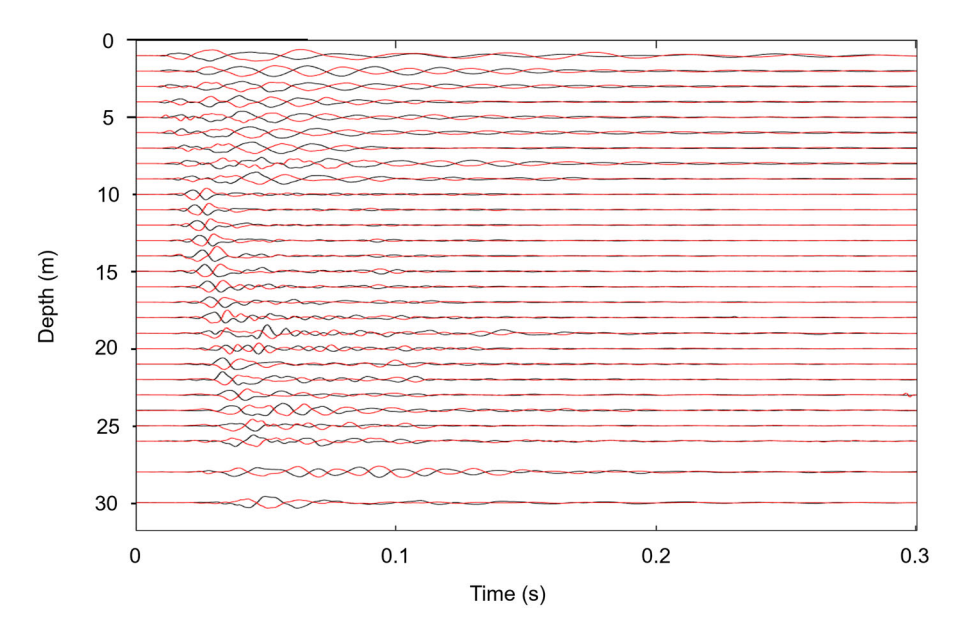


FIGURE 2 Typical waveforms acquired at different depths during downhole seismic test.

filters are often used to remove unwanted mechanical and electrical interferences from the signals, thereby improving the selection of arrival times.

The MASW survey (Park et al., 1999; Xia et al., 1999) is a seismic method used to evaluate the low-strain subsurface properties by utilizing the dispersive nature of the Rayleigh waves.  $V_{\rm S}$  profile in subsurface is determined by the inversion process and the selection of a dispersion curve between phase velocity and frequency of acquired Rayleigh waves. Typical MASW wave form

data, dispersion curve and shear wave velocity profile is shown in Figure 3. Xia et al. (1999) demonstrated that  $V_{\rm S}$  relies on the dispersion of the Rayleigh wave within the subsurface layered material. Nevertheless,  $V_{\rm S}$  estimations derived from dispersion curves using surface waves are heavily influenced by scattered and non-source-generated surface waves, body waves and higher-mode surface waves (Park et al., 1998). Due to its efficiency and ability to cover large areas with limited borehole data, MASW has become a valuable tool

18730604, 2025, 3, Downloaded from https://onlinelibrary.wiley.com/doi/10.1002/nsg.70009 by Anbazhagan Panjamani

The Librarian

, Wiley Online Library on [21/05/2025]. See the Terms

conditions) on Wiley Online Library for rules of use; OA articles are governed by the applicable Creative Commons

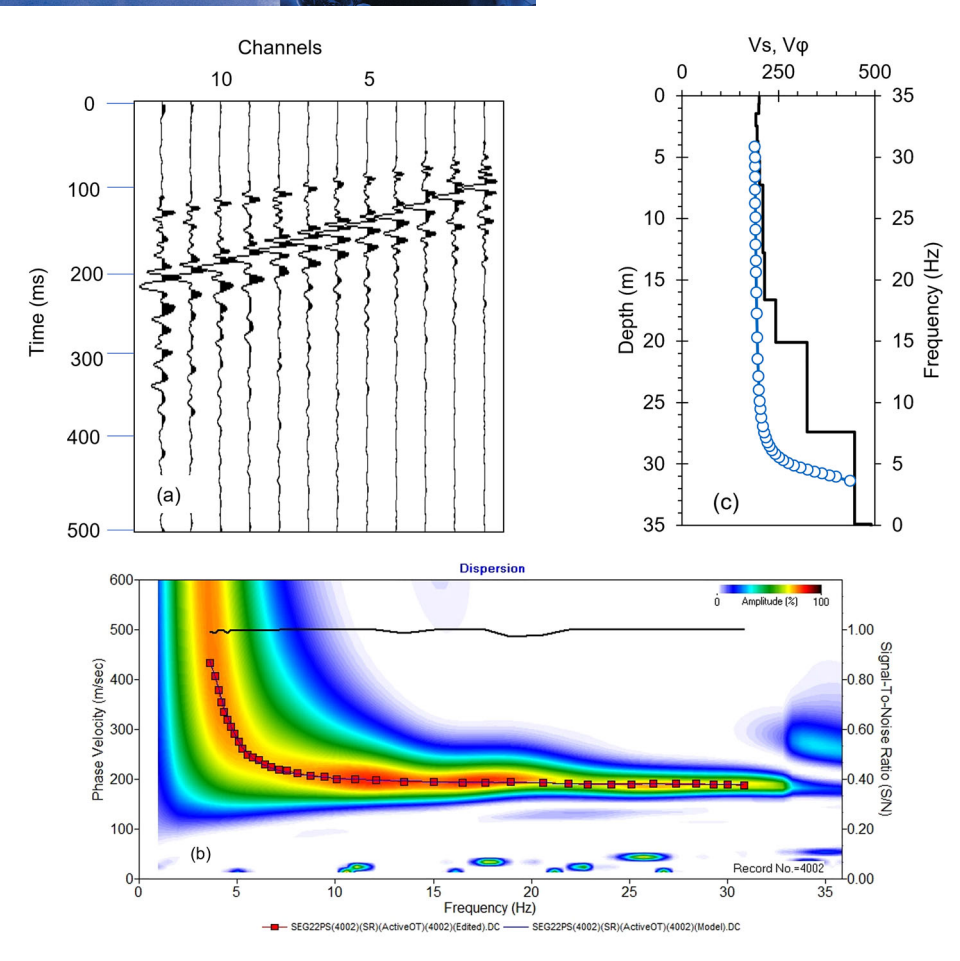


FIGURE 3 (a) Typical waveforms acquired during MASW test, (b) dispersion image and dispersion curve and (c) V<sub>S</sub> profile after inversion, at test location N1.

in geotechnical and geophysical engineering projects. Among the seismic waves, the Rayleigh waves provide the mode with the highest energy among the various waves generated during impact (Park et al., 1999; Xia et al., 1999). The MASW method typically involves three steps: (1) data acquisition; (2) dispersion curve estimation; and (3) inversion for modal parameters. Both active and passive sources can be used to generate surface waves. Active MASW employs artificial sources like sledgehammers, whereas passive MASW utilizes ambient noise. In this study, a 24-channel Geode seismograph and an array of 12 or 24 vertical geophones with 2 Hz or 4.5 Hz natural frequency were used to record surface waves. The geophones were spaced 1 m apart in a linear array, with a source offset ranging from quarter to half the array length. A sledgehammer with a metal plate served as the active source.

### DATA REDUCTION TECHNIQUES FOR DOWNHOLE TEST

The DH method estimates the velocity of body waves in different subsurface layers by measuring the arrival time

of waves from the source on the surface to the receiver to different depths in one borehole. As discussed in the previous section, the S-wave arrival is determined by the reversal of the polarity of the S-wave. This analysis is done using the crossover method, where two signals of opposite polarity are overlapped and visualized together. The arrival time is determined by the onset of a 'bow' or 'butterfly' pattern in the combined plot of the two signals, along with an increase in amplitude and a decrease in frequency (D7400-19, 2019). After arrival times for all the acquisition depths are estimated, a graph between depth and the arrival times is plotted, also known as a waterfall plot. With time, several methods have been developed to determine the  $V_{\rm S}$  profile using travel times (Bang et al., 2014; Joh & Mok, 1998; Kim et al., 2004); a few prominently used ones are the direct method (DM), interval method (IM), and refracted raypath method (RRM).

#### **Direct Method**

The DM is helpful when the source-to-borehole distance is small so the refraction through the different subsoil lay-

The Librarian, Wiley Online Library on [21/05/2025]. See the Terms

onditions) on Wiley Online Library for rules of use; OA articles are governed by the applicable Creative Common

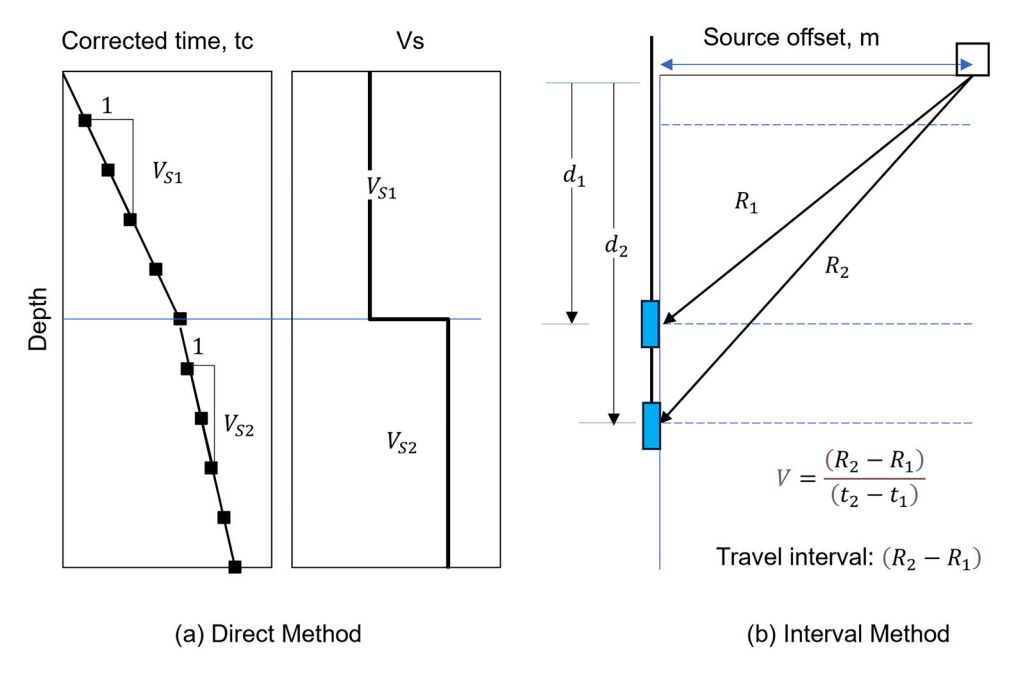


FIGURE 4 Illustration of (a) direct method and (b) interval method for downhole test analysis.

ers can be neglected. The  $V_{\rm S}$  is calculated as the slope of the travel time plot for different layers. The arrival time is corrected for depth by using Equation (1), considering that the waves travel in a straight line and no refraction occurs at the layer interfaces. Then, the slope of the corrected travel time versus depth plot is calculated as  $V_{\rm S}$ . The workflow for this method is presented in Figure 4a. This method results in an average  $V_S$  value for a soil stratum between two depths.

$$V_{\rm S} = \frac{\Delta d}{\Delta t_{\rm C}} \; ; \; t_{\rm C} = t \frac{d}{R}$$
 (1)

where  $\Delta d$  is the change in depth, and  $\Delta t_{\mathbb{C}}$  is the change in the corrected arrival time.

#### **Interval Method**

The IM considers a straight travel path from the source to the receiver.  $V_{\rm S}$  is calculated considering the difference in travel distance and travel time between the two depths (Figure 4b).

$$V_{S} = \frac{(R_2 - R_1)}{(t_2 - t_1)} \tag{2}$$

where  $R_1$  and  $R_2$  are the inclined distance to depth  $d_1$ and  $d_2$  (Figure 4b), respectively,  $t_1$  and  $t_2$  are arrival times of S-wave at  $d_1$  and  $d_2$ .

As evident, IM does not work when the travel time  $(t_1)$ up to the lower depth  $(d_2)$  is less than the travel time up  $(t_1)$  to the upper depth  $(d_1)$ , as the time difference  $(\Delta t = t_2 - t_1)$  will become negative. Moreover, IM shows

unrealistically high  $V_{\rm S}$  value when  $\Delta t$  is low, which is often observed at shallow interfaces (Bang et al., 2014; Hallal & Cox, 2019; Wang et al., 2021a). However, as it is a popular method for seismic DH data processing,  $V_{\rm S}$ and  $V_S^z$  profiles from IM are considered in the current study.

#### **Refracted Raypath Method**

The assumption of the straight raypath from the source to the receiver is valid if the  $V_S$  values of the subsurface layers are almost constant and the tests are conducted at higher depths where the travel paths become essentially vertical, so minimum refraction can occur along the raypath. However, the raypath is dependent on the  $V_{\rm S}$ values of the individual layers and bends towards the borehole with angle with vertical depending up on the V<sub>S</sub> contrast at any depth (Bang et al., 2014; Bautista & Aguilar, 2023; Kim & Park, 2002; Kim et al., 2004; Wang et al., 2021a). Figure 5 demonstrates the refraction of waves at the interface of subsurface layers and the algorithm of RRM.

The refraction at any interface is governed by Snell's Law, which relates  $V_S$  with angle of incidence and angle of refraction. First, the actual travel length  $(L_{i,i})$ in each layer is calculated based on boundary conditions in Equations (3) and (4). Travel time in each layer is estimated, and then  $V_{\rm S}$  is determined based on Equation (6).

$$\frac{\sin \theta_{i,1}}{V_1} = \frac{\sin \theta_{i,2}}{V_2} = \dots = \frac{\sin \theta_{i,j}}{V_j} = \dots = \frac{\sin \theta_{i,j}}{V_i}$$
(3)

EAGE

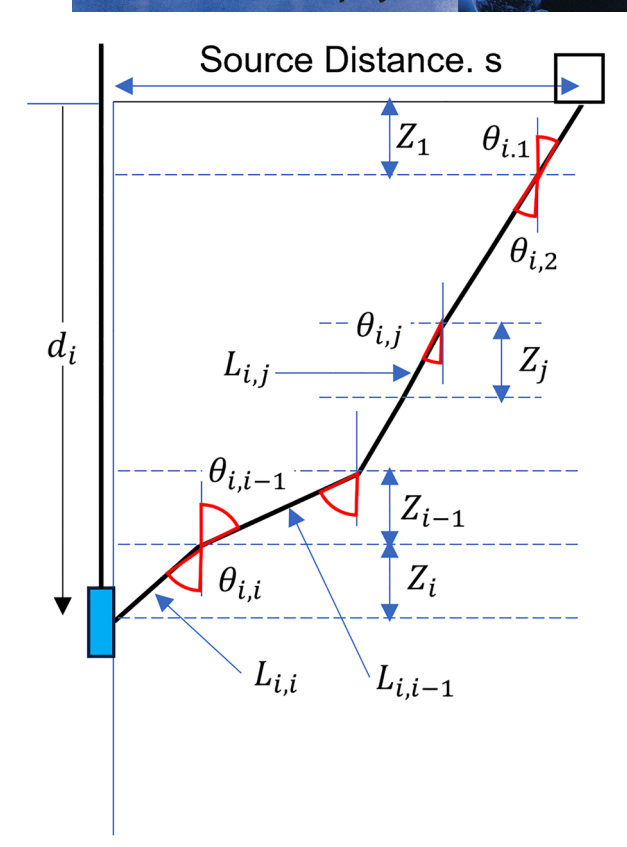


**FIGURE 5** Illustration of refracted raypath method for downhole test analysis.

$$Z_1 \tan \theta_{i,1} + Z_2 \tan \theta_{i,2} + \dots + Z_j \tan \theta_{i,j} + \dots + Z_i \tan \theta_{i,i} = s$$
(4)

$$L_{i,j} = \frac{Z_j}{\cos \theta_{i,j}} \tag{5}$$

$$V_{i} = \frac{L_{i,i}}{t_{i,i}} = \frac{\frac{Z_{i}}{\cos \theta_{i,i}}}{t_{i} - \sum_{1}^{i-1} \frac{L_{i,j}}{V_{i}}}$$
(6)

where  $L_{i,j}$  is the length of travel path for  $i^{th}$  receiver in  $j^{th}$  layer,  $t_{i,j}$  is the time of travel along raypath for the  $i^{th}$  receiver in the  $j^{th}$  layer and  $\theta_{i,j}$  is the Angle with vertical for  $i^{th}$  receiver's raypath in  $j^{th}$  layer

To start with these equations, first, an initial value of  $V_i$  needs to be assumed, which can be the straight average (SA) velocity given by  $V_i = R_i/t_i$  ( $R_i$ : straight line distance from source to receiver,  $t_i$ : arrival time of wave from the source to the receiver). These equations are solved by iteration.  $V_i$  is updated after every iteration. The iteration is continued by using the estimated  $V_i$  as input for the next iteration till the difference between the assumed and the calculated velocity at the step reduces below the defined lower limit (e.g., 0.001 m/s) (Kim et al., 2004; Kumar & Anbazhagan, 2023). RRM was improved further by incorporating the correction

for source offset using the corrected travel length after refraction (Bang et al., 2014). This helped in further reducing the fluctuations in the  $V_S$  profiles due to presence of thin layers of high or low stiffness in the profile, as observed in study conducted in predominantly alluvial deposits with little variation in subsurface lithology (Bang et al., 2014). Boore and Thompson (2007) studied different algorithms to determine subsurface interfaces to model slowness profiles and observed that the site amplifications are not prone to the rapid fluctuations in the slowness profiles at frequencies lower than 5 Hz. The site amplification at frequencies higher than 5 Hz are sensitive to subsurface model selection, which is important for engineering applications requiring design at higher frequencies corresponding to shallow depths. That means average  $V_S$  profiles in the shallow depth are also sensitive to subsurface model selection, which defines  $V_{\rm S}$  values between different interfaces. In this study, DH data from test locations at different geological settings was analysed for estimation of  $V_{\rm S}$  profiles and  $V_S^z$  up to 30 m, sediment depth and bedrock depth. The lithological log or the borelogs showed a specific delineation of the subsurface layers, which were not reflected in the trends in the travel time-depth plot. At many locations, intermittent high or low stiffness layers of varying thickness were observed, which increase the complexity of accurate  $V_{\rm S}$  profile determination. However, these were observed to influence the  $V_S^Z$  profiles only marginally. As discussed in the next section, a straight-line travel path and a single travel time measurement without considering refraction at any interface were successful in determining  $V_S^z$  with significant accuracy.

# USE OF TOTAL TRAVEL TIME TO DETERMINE AVERAGE $V_{\rm S}$ ( $V_{\rm S}^{\rm z}$ )

SA velocities are calculated directly using time and distance from the source (i.e.,  $V_S^z = R_z/t_z$ ). These are considered accurate when the soil properties for the layer between the source and the receiver are constant (to neglect refraction). SA velocities are generally more reliable at greater depths and smaller source radial offsets, as the impact of refraction becomes less of an issue (D7400-19, 2019). However, in a sense, this expression represents average velocity over the wave travel path, as it is the ratio of total travel length to the total travel time. Hence, the average velocity of the subsurface from the surface to the depth of the record can be calculated as SA velocity, which is helpful for foundation design, stiffness calculation and site classification studies where only average velocity is the required input. SA velocity straight travel path from source to receiver. However, the actual travel path is influenced by the subsurface V<sub>S</sub> contrasts, and refractions do occur along the travel path. Hence, a comparison of the  $V_S^z$  estimated

using straight and refracted raypath is studied in later sections.

#### AVERAGE V<sub>S</sub> UP TO SEDIMENT DEPTH, BEDROCK DEPTH AND V<sub>s</sub><sup>30</sup>

Average velocity and the ratio of velocities are extensively used for seismic site classification to evaluate site amplification and the response of soil during an earthquake. Even though the ratio of soil and bedrock velocity was correlated with seismic amplification,  $V_{\rm S}^{30}$ became more popular due to the international code of practice (Anbazhagan et al., 2018). So,  $V_8^{30}$  has been established as an essential parameter for seismic site classification and site response studies, where it is used to estimate site amplification factors.  $V_8^{30}$  was initially introduced to provide unambiguous definitions of site classes and site coefficients for estimating sitedependent response spectra (Borcherdt, 1994).  $V_{\rm S}^{30}$  is calculated by dividing 30 m by total travel time from 30 m depth to the surface, as shown in the following equation:

$$V_{\rm S}^{30} = \frac{30}{tt_i} = \frac{30}{\sum \frac{dd_i}{V_i}}$$
 (7)

where  $tt_i$  is the travel time from  $i^{th}$  depth to the surface or vice versa,  $dd_i$  is the thickness of the  $i^{th}$  layer and  $V_{\rm S}$  is the  $V_{\rm S}$  of the  $i^{th}$  layer.

Estimation of  $V_S^{30}$  generally requires the determination of  $V_S$  of all the layers up to 30 m and then using Equation (3). However, if the travel time up to 30 m depth is already known from the DH test and the travel path length is determined from geometry,  $V_{\rm S}^{30}$  can be directly estimated using only one reading quickly rather than measuring each layer and then calculating the average. However, there is no experimental proof of this.

Recently, limitations of  $V_S^{30}$  as a sole parameter for site classification and amplification studies have been discussed in the literature (Bajaj & Anbazhagan, 2023; Castellaro et al., 2008). Instead of  $V_{\rm S}^{30}$  alone, average  $V_{\rm S}$  up to the bedrock depth ( $V_{\rm S}^{\rm BR}$ ) and sediment depth ( $V_{\rm S}^{\rm ST}$ ) in integration of  $V_{\rm S}^{30}$  have been proposed as a better criterion for amplification and site class studies in shallow bedrock regions (Bajaj & Anbazhagan, 2023; Ghione et al., 2023). All the test locations can be considered to consist of three types of subsurface strata: sediment, weathered rock and bedrock. Sediment depth is the depth at which sediment stratum ends and weathered rock begins; bedrock depth is the depth at which bedrock starts. Site response studies have been conducted to estimate the optimum depth for input motion to revise site class provisions. The influence of sediment depth and bedrock depth have been extensively

analysed in detail in the literature (Baiai & Anbazhagan. 2023; Castellaro et al., 2008; Wu et al., 2020). Different  $V_S$  ranges have been suggested for depth of input motion. However, as the interface of sediment column and the rock strata is still considered a major impedance contrast in the subsurface geology, sediment depth and bedrock depth have been considered, and rock strata with fair rock quality designation (RQD) (Deere & Deere, 1988) values of 50 or more are adopted as Bedrock in this study. Any rock stratum with RQD < 50 is considered weathered rock layer. Hence,  $V_{\rm S}^{\rm BR}$  considers the travel path up to the bedrock depth through the weathered rock layer. For example, at test location CTR1, sediment depth is observed from borelog to be 11.3 m, whereas the bedrock depth is found to be 28.5 m. Hence,  $V_{\rm S}^{\rm ST}$ will be estimated from surface up to 11.3 m depth and Sediment depth and bedrock depth will be same for any location where a weathered rock stratum is absent. The calculation for  $V_{\rm S}^{\rm BR}$  and  $V_{\rm S}^{\rm ST}$  is same as  $V_{\rm S}^{\rm 30}$ , shown in Equation (7).

#### **CURRENT STUDY AND TEST LOCATIONS**

DH and MASW tests were conducted at five cities across varying geological formations in India. Chennai is situated on the eastern coast of India at the boundary of the Eastern Ghats and Southern Granulitic Terrain. The city's subsurface consists of alluvial and fluvial deposits, followed by Charnockite and Shale rocks. There are three test sites in Chennai: underlain by a mix of sand and clay layers, underlain by fractured rock, and hard shale rock. Coimbatore lies at the boundary of Dharwad Craton and Southern Granulitic Terrain, and most of the city consists of near-surface bedrocks of Charnockite rocks. The three test sites in the city consist of shallow near-surface bedrock consisting of limestone and Charnockite rocks. The soil layers consist of primarily sandy and silty soils.

Mangalore is a coastal city along the Western Ghats in Dharwad Craton. Lateritic deposits and sandy soil characterize the city. There are two test locations in Mangalore, one near the river, with silty sand layers followed by a thick clay stratum in the subsurface, underlain by gneiss rock. The second site consists of lateritic soil, followed by gneiss rock deposits. Bhubaneshwar lies in the eastern coastal plains alongside the Eastern Ghats, surrounded by several riverbeds. Most of the subsurface consists of riverine alluvial deposits, with a few occurrences of cemented lateritic deposits. The five test sites in Bhubaneshwar show a mix of geology with near-surface bedrock and relatively deeper sedimentthick regions. The areas close to the river show thicker sediment deposits. The southern part of the city consists of shallow lateritic and sandstone deposits. Hence, deep

and Conditions

on Wiley Online Library for rules of use; OA articles are governed by the applicable Creative Commons

soil sites at Narora town, located in the Indo-Gangetic basin in northern India with a complex subsurface formation of sandy and clayey alluvium deposits, are included in the study. There are five test sites in this town near the river Ganga. The test was conducted at all locations up to 30–35 m depth.

#### **ANALYSIS OF DOWNHOLE TEST DATA**

The arrival times of SH waves at different depths were calculated using the crossover method, as discussed previously, and a depth-time waterfall plot for each location was generated. Then, the arrival time and inclined distance of the straight raypath were used to calculate the direct  $V_{\rm S}$ , which is also the average  $V_{\rm S}$  over the entire travel path distance. Then, based on the available borelog and contrasts observed in the interval  $V_{\rm S}$ profile, the DM was used to determine the average  $V_{\rm S}$ profiles for different layers. Next, V<sub>S</sub> profiles were estimated using IM. In case of a negative  $V_S$  value,  $V_S$  from the previous depth was taken for the current depth as well. The arrival times were fed into the refracted raypath algorithm and  $V_{\rm S}$  was determined. Further,  ${V_{\rm S}}^{30}$ ,  ${V_{\rm S}}^{\rm BR}$  and  ${V_{\rm S}}^{\rm ST}$  were estimated using the determined V<sub>S</sub> profiles at each location. Raypath length for straight travel path and refracted travel path were calculated and compared to assess the differences in estimates of travel path length and error in average  $V_{\rm S}$  estimation. For V<sub>S</sub> model obtained from DM, raypath length was calculated considering the refractions at the model interfaces. Hence, even though DM considers a straight inclined raypath, a refracted raypath specific for the  $V_{\rm S}$  model is considered here and is discussed in the next section. For IM, the raypath remains straight and is the same as the straight average method (SAM). Figure 6 shows a description of the workflow for this exercise. Thereafter,  $V_{\rm S}$  profiles from MASW were compared with the  $V_{\rm S}$  profiles from DH tests. Another important aspect of DH data reduction using waterfall plots of travel time and depth is determining the interface depths of the subsurface layers. Although the borelogs provide firsthand information about the subsurface layers, these are mostly visually interpreted and do not necessarily reflect the changes in stiffness, especially if the changes in properties between layers are gradual and not sudden. A change in subsurface lithology may not indicate a change in stiffness, which often leads to ambiguity about the depths of the interfaces (Bang et al., 2014; Boore & Thompson, 2007). Hence, in this study, interfaces are delineated using the arrival times from the waterfall plot. Further, the influence of considering borelog based layers and determining the number of layers using the DM is also presented. The error in arrival time determination is also examined, and its influence on average  $V_{\rm S}$  by considering an error of ±0.50 ms is presented.

#### **RESULTS AND DISCUSSIONS**

# $V_{\rm S}$ profiles, $V_{\rm S}^{\ z}$ profiles and raypaths for test locations

Waterfall plot,  $V_S$  profiles,  $V_S^z$  profiles and raypath plots for test locations C7, BBSR1, CTR1, M1 and N1 are presented in Figures 7–11, respectively. Similar plots for all the other test locations can be accessed in supplementary material. MASW survey results in  $V_S$  profiles, which are an indication of the average  $V_S$  of a layer thickness over a global spread at a site and is commonly used to determine  $V_{\rm S}^{30}$  and site class. However, the surfacebased test gives no insight into the subsurface layers, which can only be determined using borehole-based methods. Moreover, the determination of  $V_S^z$  from DH can help remove such uncertainties in the short term, and later, a detailed profile can also be obtained using different raypath analyses, as discussed earlier. Hence, a comparison of  $V_{\rm S}$  profiles,  ${V_{\rm S}}^{30}$  and other  ${V_{\rm S}}^{\rm z}$  values, including MASW results is also discussed further. Dispersion images, dispersion curves and final velocity profiles from MASW surveys are given in Figures A2-A5.

Figure 7 shows the waterfall plot,  $V_S$  profiles,  $V_S^Z$  profiles and raypath plots for C7 location. The subsurface consists of silty clay and silty sand layers, followed by weathered shale rock and then hard shale rock. Although several layers of sand and clayey soil are visually identified from the borelog, the layers determined using the slope of linear fit between depth and corrected arrival time may not coincide with the layer boundaries from the borelog. The model using DM resulted in seven subsurface layers, of which five consist of soil. The DM results in an almost constant V<sub>S</sub> profile between 5 and 22 m (Figure 7b), below which it shows a sharp rise in  $V_S$  in weathered shale layer. The presence of almost constant  $V_{\rm S}$  profile between 5 and 22 m depth, leads to a near straight raypath between the two depths. RRM is sensitive to the actual travel length between two acquisition depths, which is reflected by the detection of two high  $V_{\rm S}$  layers at 5 m and 17 m. These  $V_{\rm S}$  values are very high for typical clayey and sandy soils. These anomalies are observed in the refracted raypath at 5 m and 17 m depth (Figure 7d,e), where the raypath moves towards the borehole and then gets refracted to a steeper path because of the velocity inversion just after the anomaly.  $V_{\rm S}$  profile from IM also results in very high  $V_{\rm S}$  values at these depths which far exceed those from RRM.  $V_S^Z$ profiles also reflect this sharp change in  $V_S$  with small bumps at these depths. In the raypath up to the sediment depth, this anomaly causes a deviation of the raypath by almost 0.5 m horizontally. Errors in total raypath length remain within 1% for most of the depths, except at 6.0 m and 7.5 m, where they are 6% and 2.3%, respectively. All the raypaths obtained from RRM up to 33 m are shown in Figure A1a. MASW results in a lower  $V_S$  values except

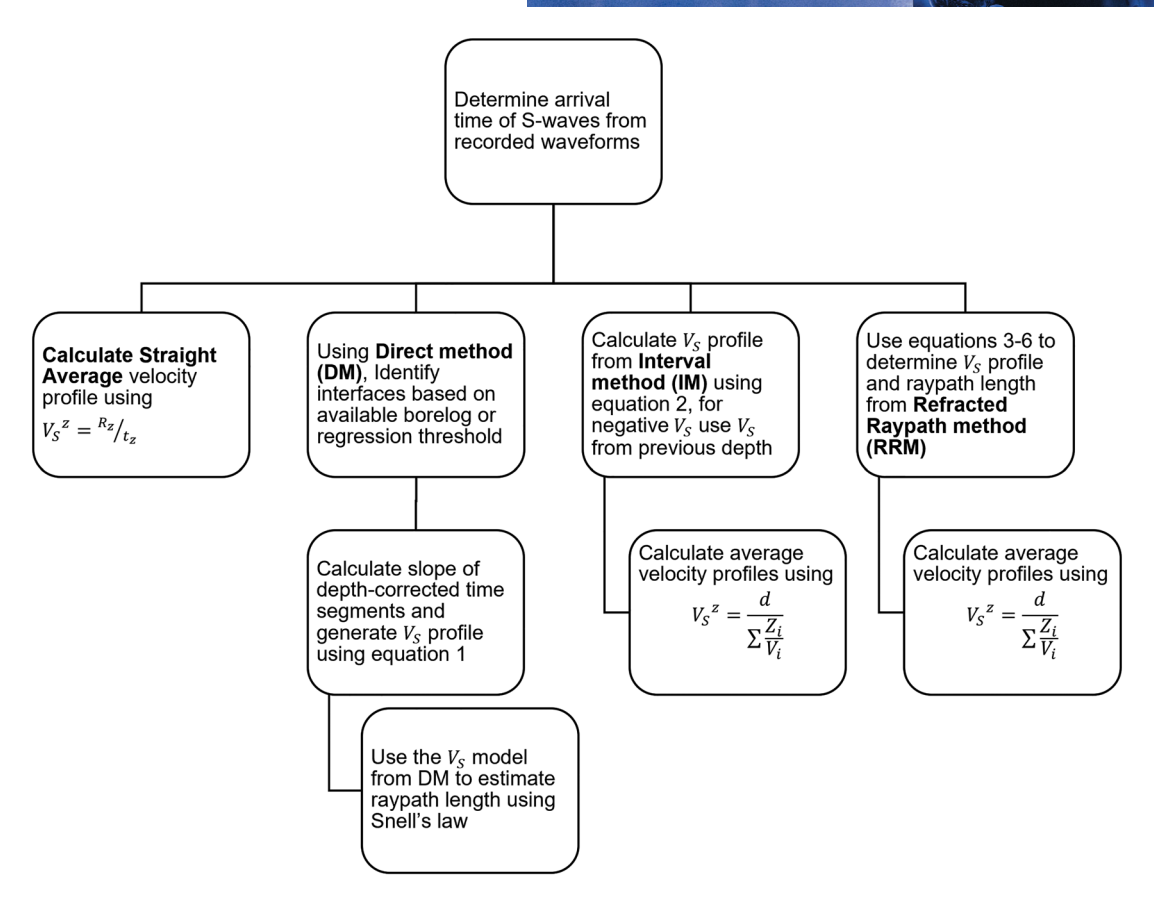


**FIGURE 6** Workflow for estimation of  $V_S$ ,  $V_S^z$  and raypath length in downhole test.

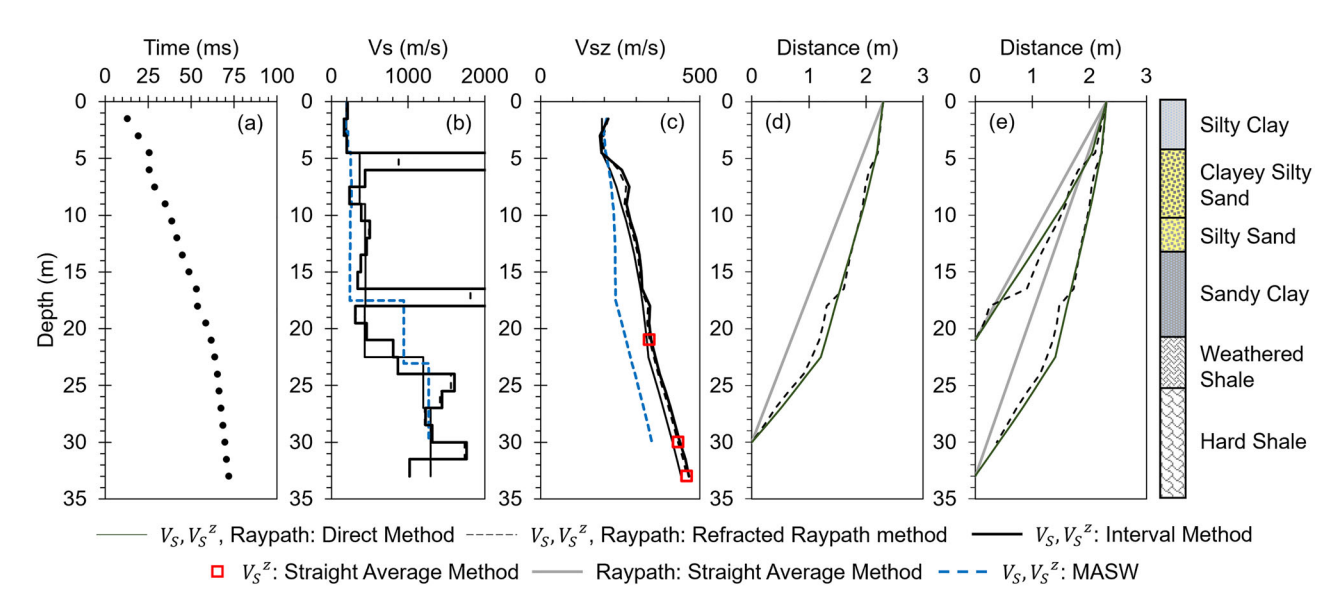
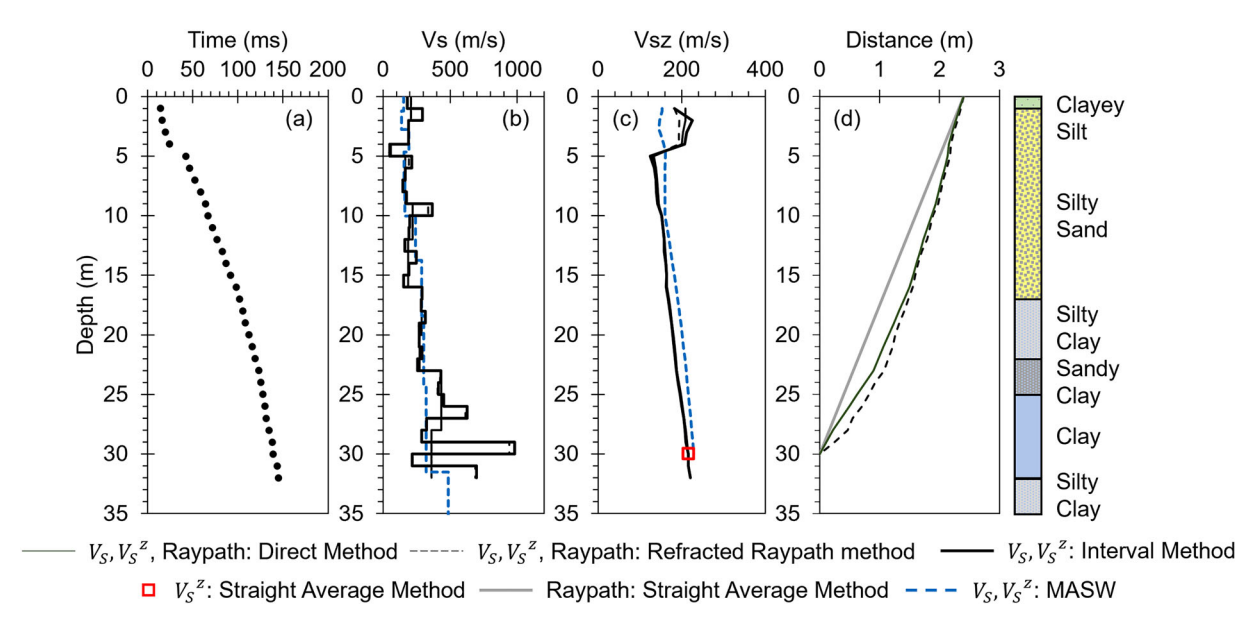


**FIGURE 7** Test location C7: (a) waterfall plot of arrival time—depth, (b)  $V_S$  profiles, (c)  $V_S^2$  profiles, (d) wave travel paths up to 30 m and (e) sediment depth and bedrock depth. Also shown is the borelog at the test site.

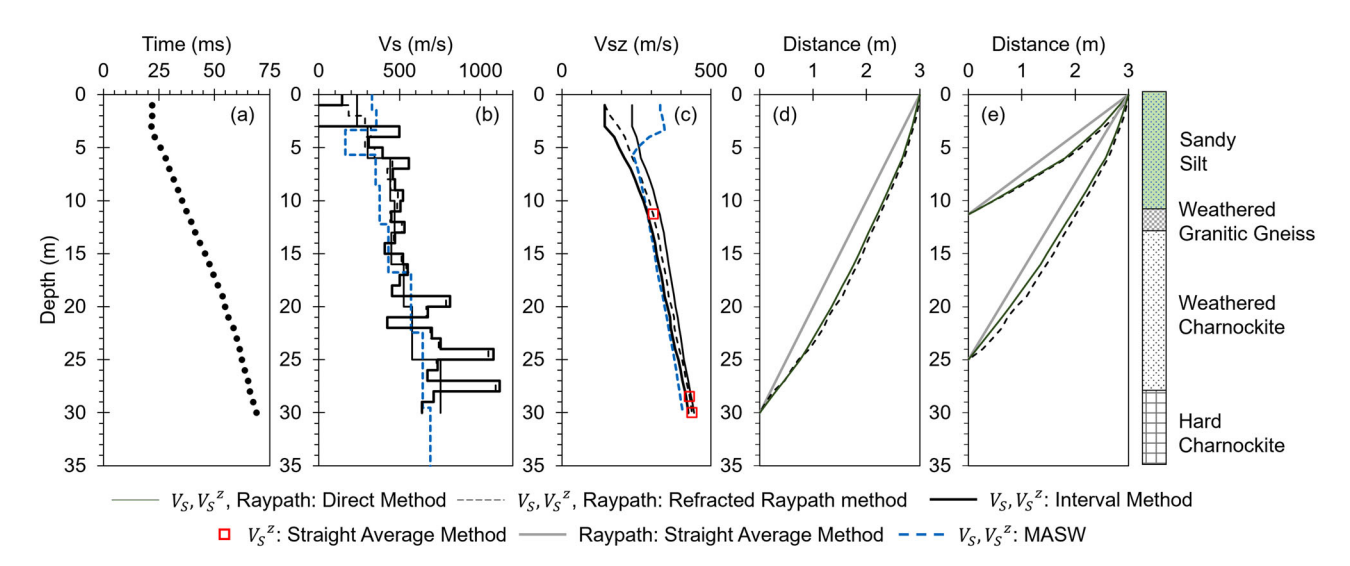
between 16 m and 24 m. The  $V_{\rm S}^{\ z}$  profile from MASW also shows lower values than the DH test (Figure 7c). The increase in  $V_{\rm S}$  from MASW is not much reflected in  $V_{\rm S}^{\ z}$  profile, as it still remains on the lower side.

Figure 8 shows the waterfall plot,  $V_S$  profiles,  $V_S^Z$  profiles and raypath plots for BBSR1 location. Based on DM, as many as 10 soil layers are identified compared to six from the borelog. The subsurface soil layers consist

, Wiley Online Library on [21/05/2025]. See the Terms



**FIGURE 8** Test location BBSR1: (a) waterfall plot of arrival time—depth, (b)  $V_S$  profiles, (c)  $V_S^z$  profiles and (d) wave travel paths up to 30 m. Also shown is the borelog at the test site.



**FIGURE 9** Test location CTR1: (a) waterfall plot of arrival time—depth, (b)  $V_S$  profiles, (c)  $V_S^z$  profiles, (d) wave travel paths up to 30 m, and (e) sediment depth and bedrock depth. Also shown is the borelog at the test site.

of silty sand and silty and sandy clays. These are low  $V_{\rm S}$  sediments, in the vicinity of the riverbed. DM model, IM and RRM result in similar  $V_{\rm S}$  profile up to 25 m, except for a marginally high  $V_{\rm S}$  layer at 10 m detected in RRM. RRM shows significant fluctuations in  $V_{\rm S}$  values towards the end of survey depth, beyond 25 m, with showing the presence of very high  $V_{\rm S}$  layers, which, however, do not influence the estimation of  $V_{\rm S}^{z}$ . Error in total raypath length remains within 1% up to the bottom of the borehole and attains a maximum of 0.6% at 6 m depth. All the raypaths obtained from RRM up to 32 m are shown in Figure A1b. DM model, IM and RRM end up in simi-

lar  $V_{\rm S}^{\ z}$  values except in shallow depths under 5 m. As the  $V_{\rm S}$  values are almost similar for most of the survey depth; the raypaths for both the reduction methods coincide till 15 m, below which the deviation in path is observed. MASW survey resulted in a  $V_{\rm S}$  profile similar to the profile from DH test. However, because the DH profiles show a low  $V_{\rm S}$  layer at 5 m depth, which is not reflected in MASW, the  $V_{\rm S}^{\ z}$  profile from MASW is marginally higher than from the DH.

Figure 9 shows the waterfall plot,  $V_S$  profiles,  $V_S^z$  profiles and raypath plots for CTR1 test location. Eight subsurface layers are identified from DM, with four of

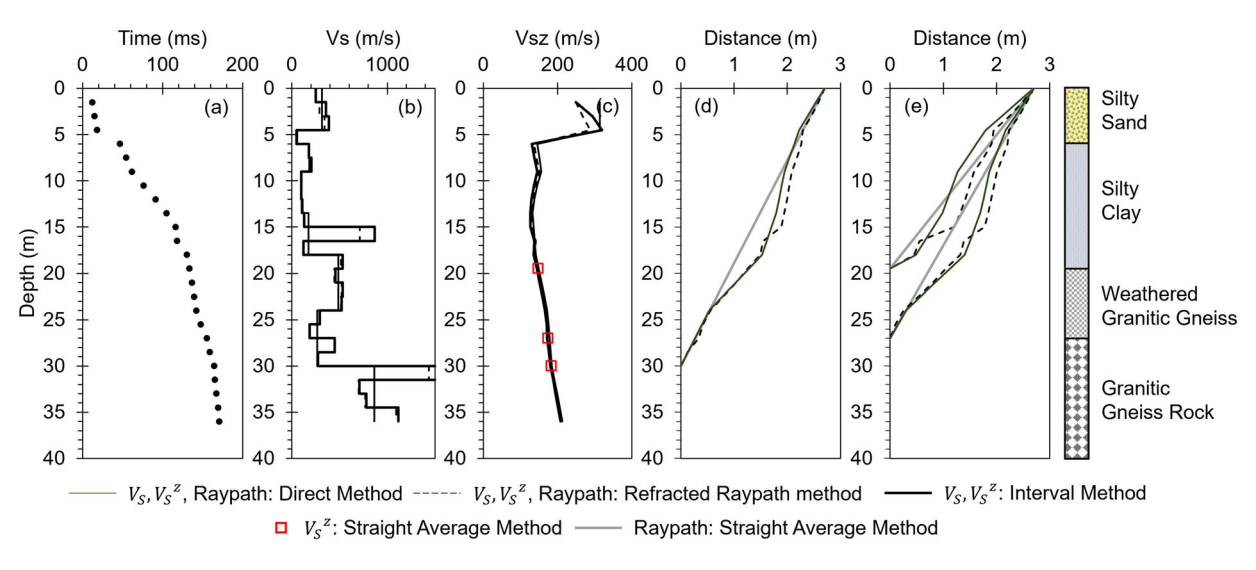


**FIGURE 10** Test location M1: (a) waterfall plot of arrival time—depth, (b)  $V_S$  profiles, (c)  $V_S^z$  profiles and (d) wave travel paths up to 30 m. Also shown is the borelog at the test site.

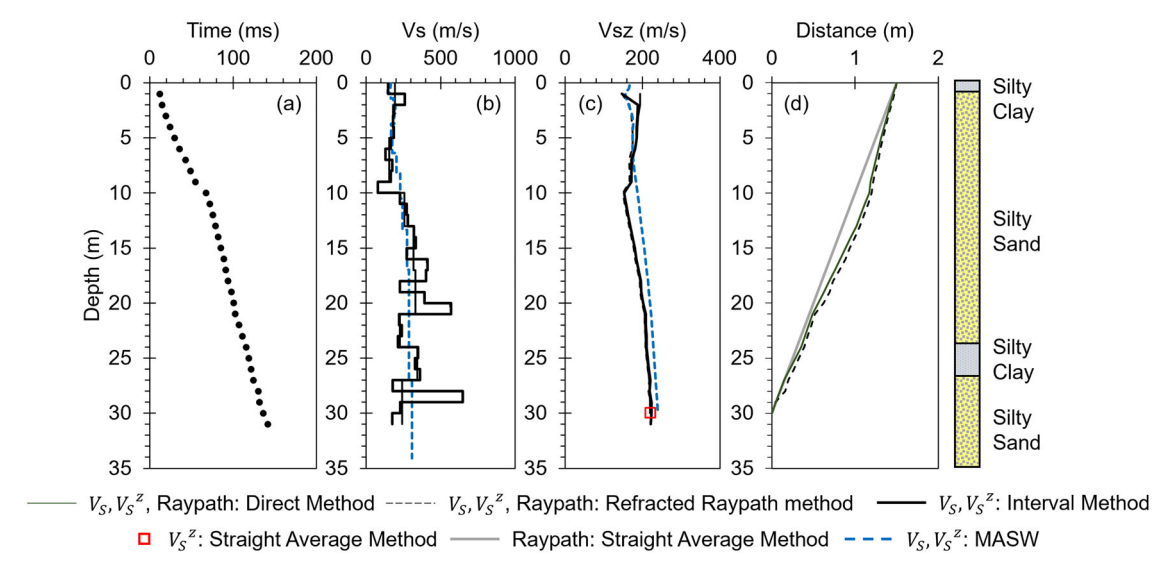


**FIGURE 11** Test location N1: (a) waterfall plot of arrival time—depth, (b)  $V_S$  profiles, (c)  $V_S^z$  profiles and (d) wave travel paths up to 30 m. Also shown is the borelog at the test site.

them in the weathered Charnockite rock layer, finally resulting in a gradually increasing  $V_{\rm S}$  profile. RRM also follows the same up to 19 m, after which there are several  $V_{\rm S}$  contrasts observed. IM results in negative  $V_{\rm S}$  values for 2 and 3 m depth and overestimated  $V_{\rm S}$  at 4 m depth (Figure 9b). The negative  $V_{\rm S}$  in the profile is replaced with  $V_{\rm S}$  of previous layer for the calculation of  $V_{\rm S}^{~\rm Z}$ . The  $V_{\rm S}^{~\rm Z}$  profile shows higher values in DM model, however, beyond 20 m, both the reduction methods show a similar range of  $V_{\rm S}^{~\rm Z}$  values (Figure 9c).  $V_{\rm S}^{~\rm Z}$  from IM is lowest of the three methods because of low  $V_{\rm S}$  in the shallow depths. As, the  $V_{\rm S}$  profile in up to 20 m does not have many fluctuations in  $V_{\rm S}$  values, the raypath up to the sediment depth coincides for both DM and RRM mod-

els. However, for raypath up to bedrock, some deviations are observed between 10 and 25 m. The raypath up to 30 m shows coinciding paths beyond 25 m. Total raypath length from straight path remains within 1% margin of the refracted raypath, with exceptions at 2–7 m depth, with maximum of 4.5% at 3 m depth. All the raypaths obtained from RRM up to 30 m are shown in Figure A1c. MASW results in mostly lower  $V_{\rm S}$  values, with the same observation in  $V_{\rm S}^{\rm Z}$  profiles as well.

Figure 10 shows the waterfall plot,  $V_{\rm S}$  profiles,  $V_{\rm S}^{\rm Z}$  profiles and raypath plots for M1 test location. This site is also close to a riverbed; however, the bedrock depth is shallow. The sediment deposit consists of low  $V_{\rm S}$  silty sand and silty clay layers. From visual inspection

in borelog, four distinct layers were identified, including weathered and hard granitic gneiss layers. DM model results in seven layers, with low  $V_{\rm S}$  layers between 5 and 18 m; similar observation is noted in RRM and IM, with an exception at 15 m, where a thin high  $V_S$  layer is identified (Figure 10b). The detection of high  $V_{\rm S}$  after 30 m coincides with the occurrence of a hard shale layer. The  $V_{\rm S}^{\rm Z}$  profiles from three reduction methods result in the same values beyond 5 m. Under 5 m, RRM results in lower  $V_{\rm S}$  and  $V_{\rm S}^{\rm z}$  values than DM and IM (Figure 10c). The influence of the high  $V_{\rm S}$  layer clearly is seen in the raypath diagrams, causing a significant deviation in raypath at 15 m (Figure 10d,e). The three raypath plots show that raypaths for DM model and RRM coincide beyond 18 m, and both of them coincide with straight-line raypath at 23 m. The error in total ravpath estimate using straight path assumption remains within 1%, with maximum error observed to be 1.2% at 7.5 m depth. All the raypaths obtained from RRM up to 36 m are shown in Figure A1d.

Figure 11 shows the waterfall plot,  $V_S$  profiles,  $V_S^Z$  profiles and raypath plots for N1 test location. This location consists of sandy and clayey alluvial deposits up to deep depths, which are highly prone to amplification and liquefaction due to low stiffness (Bajaj & Anbazhagan, 2023). Within 30 m depth, four layers of clay and sandy soils are identified from the borelog. However, based on the corrected time-depth plot, multiple subsurface layers are identified from DM (Figure 11b). RRM and IM show an increase in  $V_S$  after 10 m; DM model results in an almost constant  $V_{\rm S}$  profile up to 9 m, followed by a layer of lower and again higher stiffness (Figure 11b). RRM and IM identify two thin layers of higher  $V_{\rm S}$  at 20 and 29 m depth, both of which are accompanied by higher gravel content with dense sand in the borelog. Both methods result in almost coinciding raypath up to 30 m depth, with minor deviations due to the high  $V_{\rm S}$  layer at 20 m (Figure 11d). V<sub>S</sub> profile obtained from MASW almost overlaps RRM V<sub>S</sub> profile up to 6 m, after which it increases. A similar trend is observed in  $V_S^z$  profile as well. Even though the DH  $V_{\rm S}$  values are higher than MASW at many depths, the  $V_S^z$  values from MASW are higher beyond 6 m up to the survey depth (Figure 11c). Error in total raypath length estimation from straight path leads to minimal errors with maximum of 0.47% at 2 m depth. All the raypaths obtained from RRM up to 31 m are shown in Figure A1e.

It was observed that the  $V_{\rm S}$  profiles obtained from DM, IM and RRM are mostly similar, with occasional sensitivity to the time difference between two subsequent acquisition depths, where IM results in high  $V_{\rm S}$  values. The presence of high  $V_{\rm S}$  contrasts lead to noticeable changes in the travel path, as shown in Figures 7, 8 and 11. These deviations in travel path are minimal when the  $V_{\rm S}$  profiles are gradual, as the angle of incidence and angle of refraction will not be much different

to cause any sudden change in the raypath at the layer boundary. Because of refraction, the length of travel for the seismic wave is different in each layer and affects the calculation of  $V_{\rm S}$  in the inversion algorithm. The straight raypath is in general equal to the refracted raypath from source to receiver, within 1% error, which in a few cases reaches 5%–6% as well. The maximum deviation in raypath length was not necessarily confined to the first interface observed; however, it always occurred well within top 10 m, and the deviation kept reducing with depth. It can also be inferred that the maximum deviation occurs after the first major  $V_{\rm S}$  contrast, which may be an increase or a decrease in  $V_{\rm S}$ .

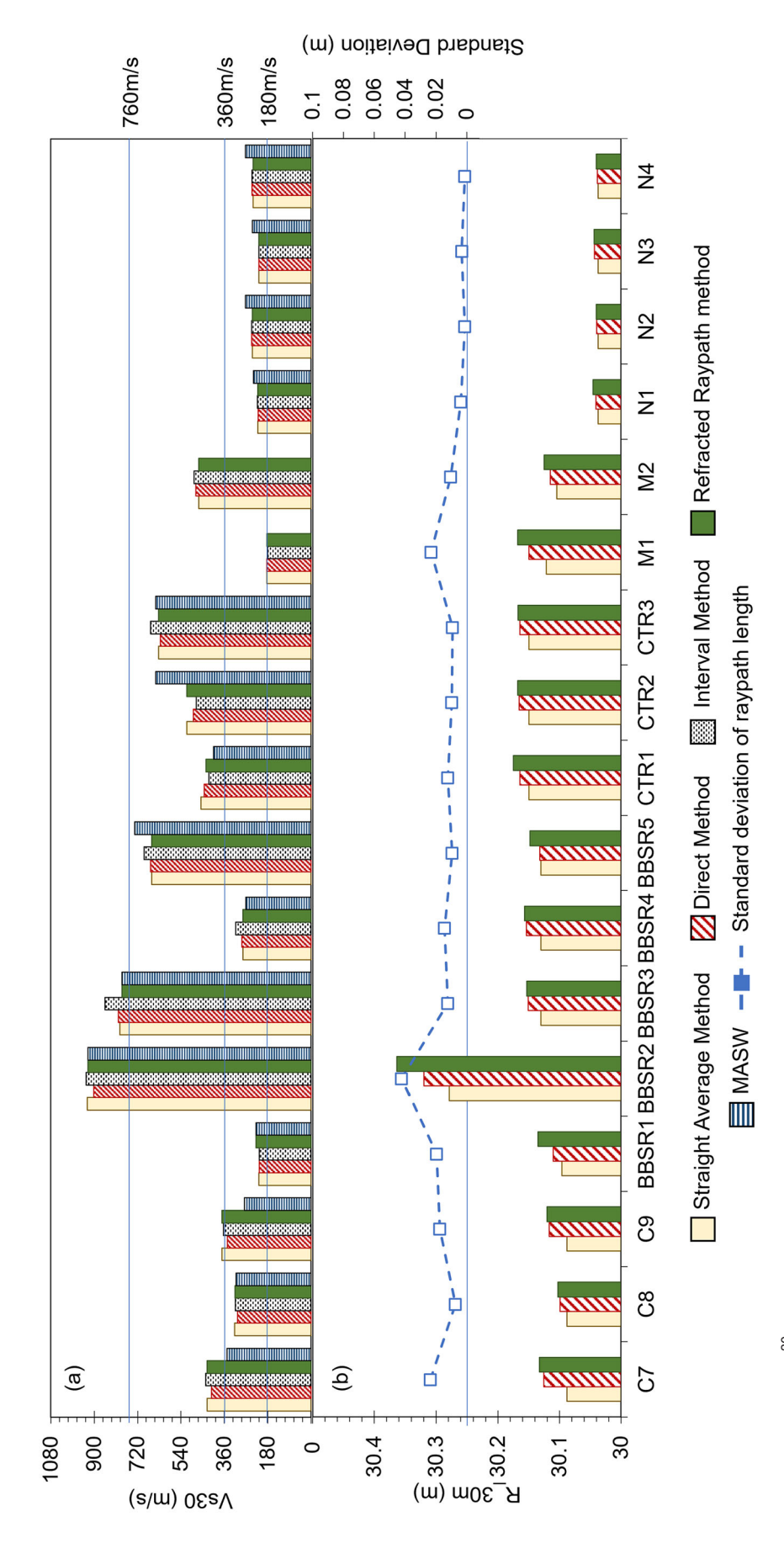
Even though the  $V_{\rm S}$  profiles from DM and RRM show high differences at a few instances, the  ${V_{\rm S}}^z$  profiles are almost collinear beyond shallow depths. The  ${V_{\rm S}}^z$  values obtained from the SAM are almost equal to the  ${V_{\rm S}}^z$  values from RRM and the DM. Similar to DM, MASW  $V_{\rm S}$  profiles do not capture a detailed variation of  $V_{\rm S}$  values in the subsurface. However, both the profiles can give a good approximation for  $V_{\rm S}$  of subsurface layers. Further, to investigate the effect of the method of  $V_{\rm S}$  estimation in average wave velocities, that is,  ${V_{\rm S}}^{30}$  or  ${V_{\rm S}}^{\rm ST}$  or  ${V_{\rm S}}^{\rm BR}$  from DH seismic test, data are presented in the next section.

## Average velocities at 30 m depth, sediment depth and bedrock depth

Shear wave velocities at all 17 locations are further used to estimate average wave velocity at varying depths  $(V_S^{30} \text{ or } V_S^{ST} \text{ or } V_S^{BR})$  and to understand the effect of direct measurement at the same depth. The assumption of a straight-line travel path results in a shorter travel path. However, the cumulative difference in refracted raypath is observed to be very small at depth beyond very shallow depths. Figure 12 presents  $V_S^{30}$  and travel path length up to 30 m depth. The standard deviation of the raypath length is also shown in Figure 12b.

As already discussed, the total length of travel remains almost equal from the three methods and remains unaffected due to the refraction and changes in layers along the travel path. Minor changes in the range of 0.05–0.1 m are found, which is even less than 0.2%. The standard deviation of the raypath length up to 30 m is within 0.05 m. Hence, even if the corrected raypath length is used for  $V_{\rm S}^{30}$  estimation, the improvement won't be more than 0.2%. Thus, the SAM is applicable to estimate  $V_{\rm S}^{30}$  at all test locations. Figure 12a shows the  $V_{\rm S}^{30}$  values obtained from the different DH reduction methods along with MASW. No significant changes in the  $V_{\rm S}^{30}$  are noted at any location causing change of the site class, except at C9, that too is observed because the  $V_{\rm S}^{30}$  values are very close to the limit between classes C and D,

onditions) on Wiley Online Library for rules of use; OA articles are governed by the applicable Creative Commons License



(a)  $V_{\rm S}^{30}$  at the test locations showing a possible misinterpretation of site class and (b) raypath length up to 30 m (bottom) along with the standard deviation implying the small scatter in the estimate. FIGURE 12

8730604, 2025, 3, Downloaded from https://onlinelibrary.wiley.com/doi/10.1002/nsg.70009 by Anbazh

, Wiley Online Library on [21/05/2025]. See the Terms and Conditions (https://onlinelibrary.wile

ns) on Wiley Online Library for rules of use; OA articles are governed by the applicable Creative Commons

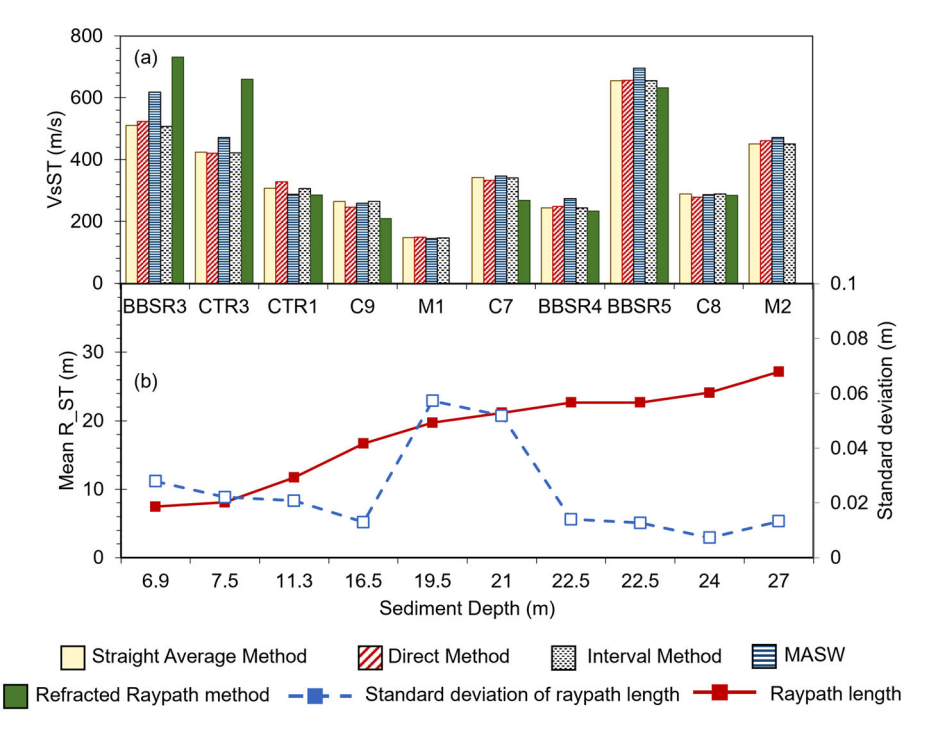


**FIGURE 13** (a)  $V_S^z$  or  $V_S^{ST}$  (b) mean raypath length up to sediment depth with standard deviation. Mean R\_ST: Mean raypath length up to sediment depth.

that is, 360 m/s. However,  $V_{\rm S}^{30}$  values from MASW show significant differences in  $V_{\rm S}^{30}$  values at a few locations, such as C7, C9, BBSR5 and CTR2. However, a change in seismic site class was observed only at C7 and C9. In general, irrespective of the differences in  $V_{\rm S}$  profiles,  $V_{\rm S}^{30}$  values from MASW match those obtained from DH tests. However, DH results may be more appropriate, as they measure shear wave velocity directly, considering the source-receiver distance.

As the study region consists of shallow bedrock sites with high impedance contrast, the application of  $V_{\rm S}^{30}$ for site classification remains ambiguous (Ghione et al., 2023), and  $V_{\rm S}$  of rock strata leads to overestimation of site class. Hence, recently average  $V_S$  up to sediment depth  $(V_S^{ST})$  and up to bedrock depth  $(V_S^{BR})$  have been introduced to better estimate site response and site class. So, similar to  $V_{\rm S}^{30}$  estimation, for the  $V_{\rm S}^{\rm ST}$  and  $V_{\rm S}^{\rm BR}$ , the range of  $V_{\rm S}^{\rm z}$  values obtained from DH for the selected locations are very narrow, and the deviation is found insignificant to interpret (Figures 13 and 14). Mean raypath lengths are calculated considering the average of raypath length obtained from the three methods. The small magnitude of scatter in the raypath length estimation from DH methods is confirmed by minimal standard deviation. Hence, the raypath length from the three models is within the accuracy of 0.130 mm. The straight raypath method is considered applicable without any significant error in  $V_S^z$  estimation up to sediment layer thickness or up to the bedrock depth.

It was observed that for both  $V_S^{ST}$  and  $V_S^{BR}$ , the DH seismic test results are better matched with the MASW results for the locations with higher sediment and bedrock dept. For the shallow rock sites, the MASW  $V_S^z$ are significantly different from DH  $V_S^z$ , with margin of error as high as 200 m/s (Figures 13 and 14), which can change site class sometimes. The study shows that if it is possible to measure directly  $V_{\rm S}$  as a part of geotechnical testing, it is more than sufficient to estimate  ${V_{\rm S}}^{30}$  or  ${V_{\rm S}}^{\rm ST}$  or  ${V_{\rm S}}^{\rm BR}$  and thereby, seismic site classification.

# Influence of error associated with arrival time detection on $V_S^2$ Profiles

Determination of arrival time of S-waves in DH test requires picking of standard signatures in the acquired waveform (D7400-19, 2019). As discussed previously, the S-wave arrival is characterized by an increase in amplitude, reduction in frequency and a bow pattern when two opposite polarized waves are superimposed. Figure 2 shows such acquired waveforms for different depths. It is difficult to estimate the exact first arrival of shear wave on signal traces, leading to introduction of errors in the velocity profiles as well. To study the effect of such uncertainties on average velocity profiles, random error of  $\pm 0.5$  ms is applied to the arrival time and then  $V_S^z$  is calculated from DM and RRM. Figure 15 shows the  $V_S$  and  $V_S^z$  profiles along with

maximum and minimum values obtained incorporating

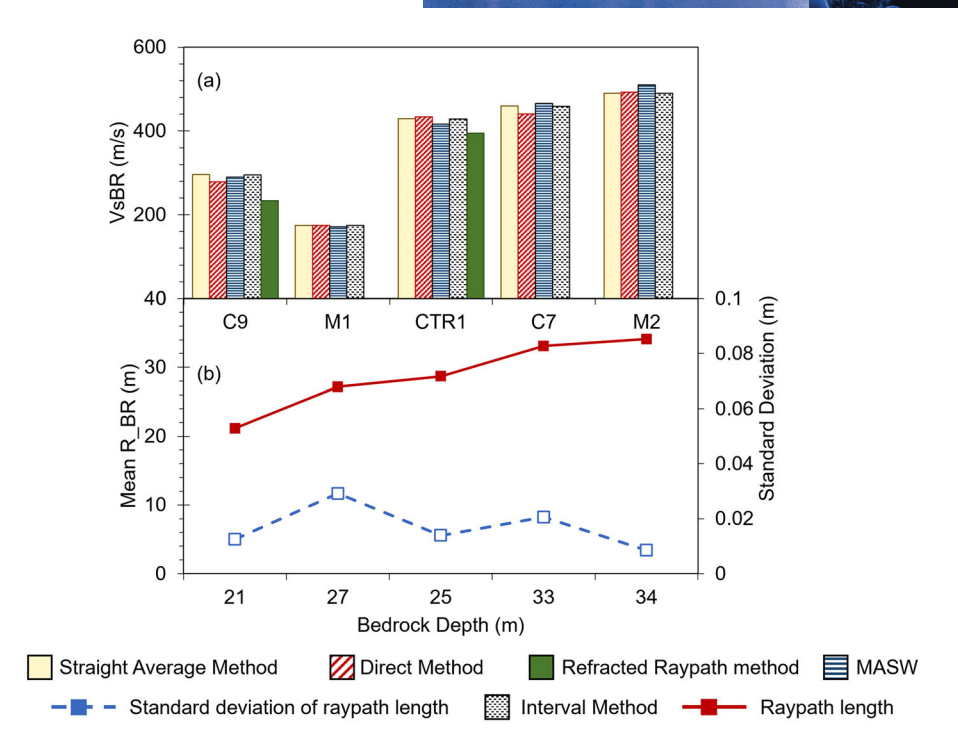


**FIGURE 14** (a)  $V_S^z$  or  $V_S^{BR}$  and (b) mean raypath length up to bedrock depth with standard deviation. Mean R\_BR: Mean raypath length up to bedrock depth.

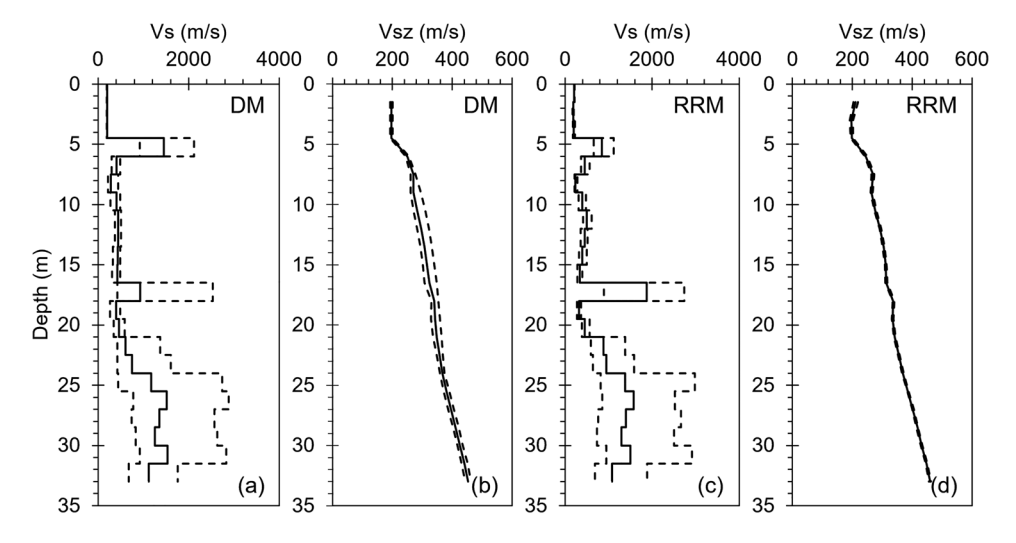


**FIGURE 15** (a)  $V_S$  profile from direct method (DM), (b)  $V_S^z$  profile from DM, (c)  $V_S$  profile from refracted raypath method (RRM) and (d)  $V_S^z$  profile from RRM, with error margins due to random error of  $\pm 0.50$  ms in arrival time at Test site C7.

the error in the arrival time at C7. It can be observed that at some depths, the  $V_{\rm S}$  profile has a high deviation, both from DM and RRM, but the uncertainty reduces extensively in  $V_{\rm S}^{\ Z}$  profiles. Overall,  $V_{\rm S}^{\ Z}$  from DM shows more variation than  $V_{\rm S}^{\ Z}$  from RRM. As,  $V_{\rm S}^{\ Z}$  involves averaging the  $V_{\rm S}$  values with depth, high  $V_{\rm S}$  in one depth has less influence on  $V_{\rm S}^{\ Z}$ . Similar findings for BBSR1, CTR1, M1 and N1 are presented in Figures 16–19, respectively. At CTR1 in Figure 13b,  $V_{\rm S}^{\ Z}$  profile shows a wider band with standard deviation of 20–25 m/s, leading to overall

band width of  $\sim$ 70 m/s around the mean  $V_{\rm S}^{\rm z}$ . At other test locations, the band for  $V_{\rm S}^{\rm z}$  is much narrower.

### Influence of model selection for downhole data reduction

One uncertainty that creeps into site response and classification studies is the determination of subsurface layer thicknesses for analysis. A model correctly demonstrat-

18730604, 2025, 3, Downloaded from https

**FIGURE 16** (a)  $V_S$  profile from direct method (DM), (b)  $V_S^z$  profile from DM, (c)  $V_S$  profile from refracted raypath method (RRM) and (d)  $V_S^z$  profile from RRM, with error margins due to a random error of  $\pm 0.50$  ms in arrival time at Test site BBSR1.

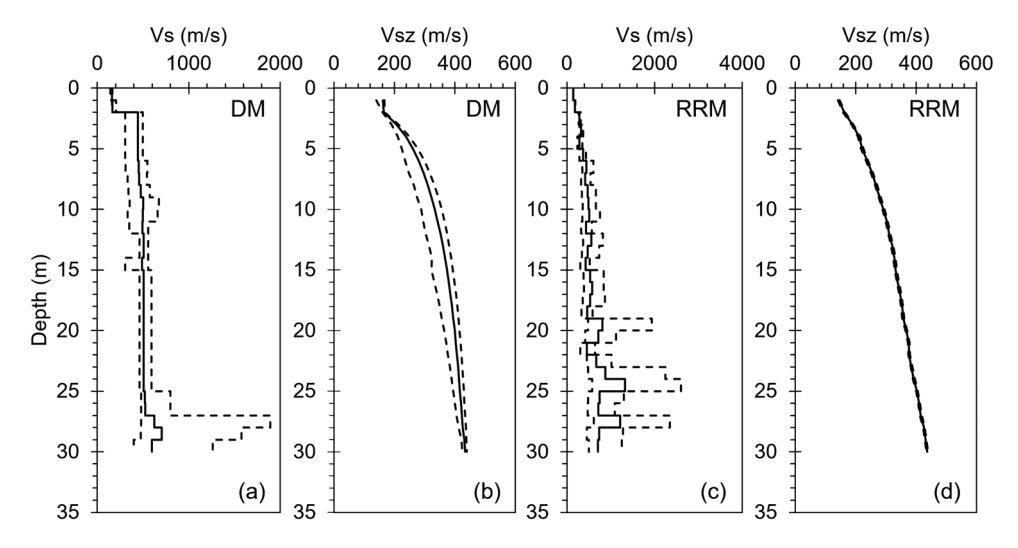


**FIGURE 17** (a)  $V_{\rm S}$  profile from direct method (DM), (b)  $V_{\rm S}^{\rm z}$  profile from DM, (c)  $V_{\rm S}$  profile from refracted raypath method (RRM) and (d)  $V_{\rm S}^{\rm z}$  profile from RRM, with error margins due to random error of  $\pm 0.50$  ms in arrival time at Test site CTR1.

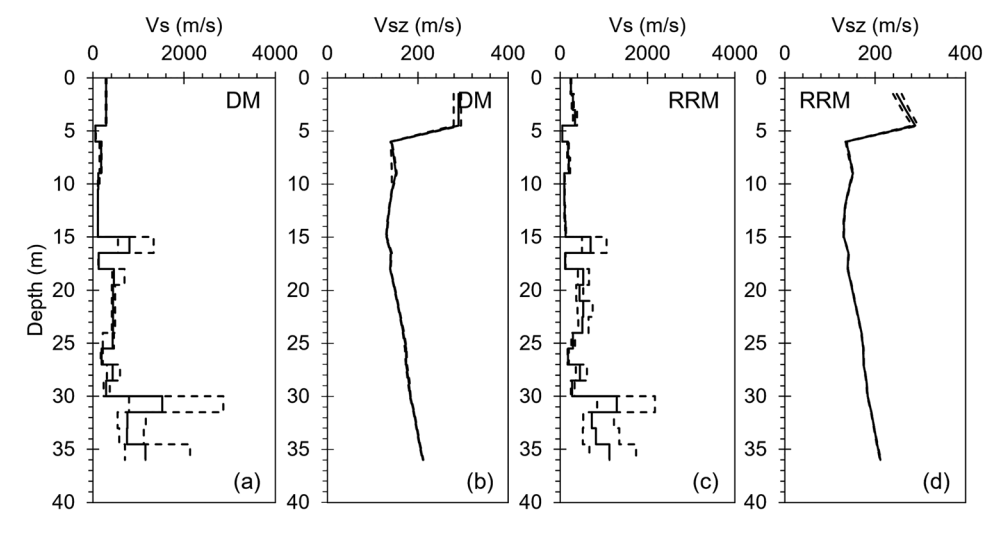


**FIGURE 18** (a)  $V_S$  profile from direct method (DM), (b)  $V_S^z$  profile from DM, (c)  $V_S$  profile from refracted raypath method (RRM) and (d)  $V_S^z$  profile from RRM, with error margins due to random error of  $\pm 0.50$  ms in arrival time at Test site M1.

on Wiley Online Library for rules of use; OA articles are governed by the applicable Creative Commons

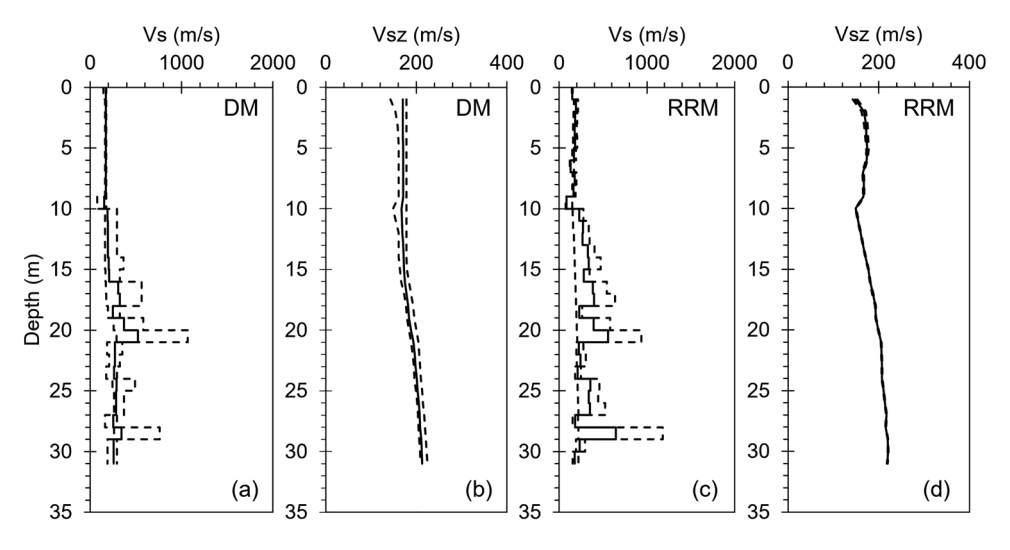


**FIGURE 19** (a)  $V_S$  profile from direct method (DM), (b)  $V_S^z$  profile from DM, (c)  $V_S$  profile from refracted raypath method (RRM) and (d)  $V_S^z$ profile from RRM, with error margins due to a random error of ±0.50 ms in arrival time at Test site N1.

ing the depths of various subsurface interfaces is often sought after for such studies. If the borelog profile is available, the distinction between the layers can be made; however, in the absence of any such log, the interpretation becomes ambiguous. In such cases, the arrival time-depth plot is used to delineate different subsurface layers for further studies. Here, test location M2 is considered to demonstrate the influence of the selection of subsurface interface depths on  $V_{\rm S}^{30}$  estimation and refracted raypath lengths. The subsurface at M2 is characterized by lateritic sediments followed by weathered and granitic gneiss rock formations (Figure 20a). Different subsurface interfaces were considered, such as borelog based interfaces and manually selected from slope of depth-corrected time plot, which led to different  $V_{\rm S}$  profiles.  $V_{\rm S}$  values vary significantly at some depths with changes in the number and depth of interfaces. V<sub>S</sub> is calculated from regression of the linear fit of the data points between two interfaces. It is important to study if these different profiles influence the site class and determination of  $V_{\rm S}^{30}$  as well.

In Figure 20a, borelog-based model, two-layer model and four-layer model are presented. Figure 20b shows the  $V_{\rm S}$  profiles and  ${V_{\rm S}}^{\rm z}$  profiles. It is observed that with increase in depth, the band of  ${V_{\rm S}}^{\rm z}$  becomes narrower, which is also visible in Figure 20c. The raypath length up to 30 m for different models is within the range of 30.1-30.15 m, which is a variation of 0.05 for 30 m depth, which again is less than 1%. Hence, the influence of model selection on  $V_{\rm S}^{30}$  will be insignificant.  $V_{\rm S}^{30}$  calculated from different models at M2 is  $460 \pm 20$  m/s except for the single layer model, which results in much higher  $V_{\rm S}^{30}$ . Hence, the selection of a model for DH data reduction has minimal influence on  ${V_{\rm S}}^{30}$  and raypath length. The same has been observed for other locations as well, where the total travel length and  ${V_{\rm S}}^{30}$  change only

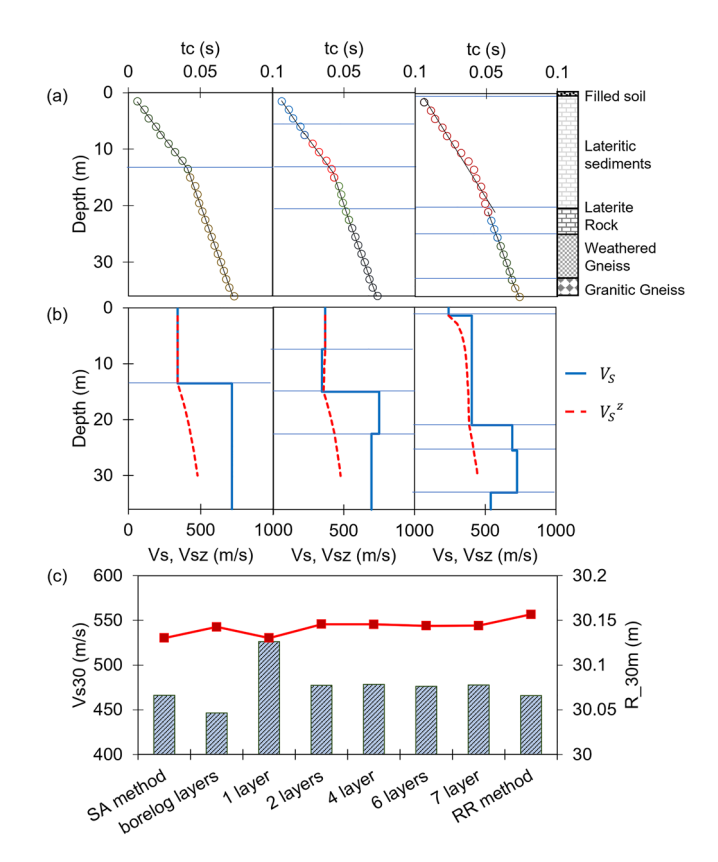


FIGURE 20 (a) Different subsurface models from corrected arrival time and depth plot at M2, shown here are two layers, four layers model and borelog based model, (b)  $V_{\rm S}\,$  profiles (solid lines) and  $V_S^z$  profiles (dashed lines) and (c)  $V_S^{30}$  estimation (columns) and Raypath length (line with square markers) up to 30 m for different models. SA, straight average.

marginally with the change in the DH reduction method; it implies that the arrival time of the S-wave at 30 m and the length of the straight travel path is sufficient to estimate  $V_S^{30}$  in the DH test. If the objective is to determine

und-conditions) on Wiley Online Library for rules of use; OA articles are governed by the applicable Creative Commons

... 30

 ${V_{\rm S}}^{30}$  for site classification purposes and a detailed subsurface layer  $V_{\rm S}$  profile is not an immediate requirement, the SAM can be used to save time and computational effort, that is, utilizing one measurement at 30 m depth to estimate  ${V_{\rm S}}^{30}$ .

#### **CONCLUSIONS**

This study employed seismic DH tests to estimate subsurface  $V_{\rm S}$  profiles. Three methods of data reduction were used to estimate  $V_{\rm S}$  profiles and further to calculate the average  $V_{\rm S}$  ( $V_{\rm S}^{\rm Z}$ ) up to 30 m, up to the sediment depth and up to the bedrock depth. The bedrock depth is considered per the RQD values obtained from the borelog, where weathered rock is considered with RQD less than 50 and bedrock with RQD exceeding 50, which is a fair quality bedrock. Moreover, the  $V_{\rm S}$  and  $V_{\rm S}^{\rm Z}$  values were compared with the results of a more commonly used MASW survey as well. Several models for  $V_{\rm S}$  profiles were studied at two locations to study uncertainty in raypath length and  $V_{\rm S}^{\rm 30}$  due to model selection. The major conclusions obtained from this study are as follows.

- 1. The travel path length obtained from the direct and RRMs up to 30 m are marginally higher than the straight raypath, which is the shortest travel path length. The total length of the travel path is minimally affected by the subsurface layering and the refractions occurring along the travel path. The standard deviation for raypath length from the three methods is estimated to be within 0.05 m, which is minimal.
- 2. When corrected for refracted raypath,  $V_{\rm S}^{\ z}$  doesn't change by more than 0.2%. Hence, the SAM can be directly used to calculate  $V_{\rm S}^{\ 30}$  by estimating the arrival time at 30 m and straight travel path length in a simple calculation, thus saving time and effort. Straight travel path assumption for average  $V_{\rm S}$  estimation can be extremely useful if the objective of the survey is site classification and seismic response prediction. Similar observations are noted for  $V_{\rm S}^{\ ST}$  and  $V_{\rm S}^{\ BR}$ . Thus, acquired data close to the soil rock interface and at 30 m can be directly utilized.
- 3. Selection of subsurface  $V_{\rm S}$  model from a given travel time-depth plot has little impact on  ${V_{\rm S}}^{30}$  value and raypath lengths are within narrow margin compared to the SAM and straight travel path.
- 4. The error associated with arrival time pickup results into highly varying  $V_{\rm S}$  profile both from DM and RRM; however, the errors in  $V_{\rm S}^{\ z}$  are marginal.
- 5. With the increase in sediment depth and bedrock depth, the  ${V_{\rm S}}^{\rm z}$  up to the bottom of the sediment layer or the bedrock layer ( ${V_{\rm S}}^{\rm ST}$  and  ${V_{\rm S}}^{\rm BR}$ ), obtained from DH tests show good agreement with  ${V_{\rm S}}^{\rm z}$  obtained

from MASW survey. In shallow depths, the difference between  $V_S^z$  from DH and MASW is large.

#### DATA AND RESOURCES

All the data used in this study was acquired in the extensive field study conducted across India. Further processing was performed using MATLAB package (https://in.mathworks.com/products/matlab.html) and crossover plot toolbox (https://geotomographie.de/). The processed data and profiles used for analysis in this study are presented in the plots in the figures and will be made available on reasonable request. Supporting Information section for this article includes plots for depth time,  $V_{\rm S}$ ,  $V_{\rm S}^{\rm Z}$  and raypaths at the other 12 test locations.

#### **ACKNOWLEDGEMENTS**

The authors gratefully acknowledge the contributions of Harish Thakur, Kamalhassan, Ravinesh Kumar and Siriwanth Kumar for their invaluable assistance in field testing. The authors also thank Sauvik Halder and Divyasree V for their contribution in data processing. This study was greatly benefitted by technical support from Dr. Thomas Fechner of Geotomographie GmBH, and the authors thank him and his team.

#### DATA AVAILABILITY STATEMENT

The data that support the findings of this study are available from the corresponding author upon reasonable request.

#### ORCID

Anbazhagan Panjamani https://orcid.org/0000-0001-9804-5423

#### **REFERENCES**

- Anbazhagan, P., Kumar Katukuri, A., Reddy, G.R., Moustafa, S.S.R. & Al-Arifi, N.S.N. (2018) Seismic site classification and amplification of shallow bedrock sites. *PLoS ONE*, 13(12), e0208226, https://doi. org/10.1371/journal.pone.0208226.
- Areias, L. & Van Impe, W.F. (2006) Effect of travel path in the SCPT test method. In: Site and geomaterial characterization, Reston, VA: American Society of Civil Engineers, pp. 236–242. https://doi.org/10.1061/40861(193)30
- Bajaj, K. & Anbazhagan, P. (2023) Effective input velocity and depth for deep and shallow sites for site response analysis. *Geomechan-ics and Geoengineering*, 18(3), 193–207, https://doi.org/10.1080/ 17486025.2021.2023766.
- Bang, E.S., Cho, S.J. & Kim, D.S. (2014) Mean refracted ray path method for reliable downhole seismic data interpretations. *Soil Dynamics and Earthquake Engineering*, 65, 214–223, https://doi. org/10.1016/j.soildyn.2014.06.009.
- Bautista, P. & Aguilar, Z. (2023) Interpretation methods for seismic downhole test in inclined boreholes. *Civil Engineering Journal*, 9(10), 2592–2611, https://doi.org/10.28991/CEJ-2023-09-10-016.
- Boore, D.M., Gibbs, J.F. & Joyner, W.B. (2021) Damping values derived from surface-source, downhole-receiver measurements at 22 sites in the San Francisco bay area of central California and the San Fernando valley of southern California. *Bulletin of the Seismologi*-

and Conditions

on Wiley Online Library for rules of use; OA articles are governed by the applicable Creative Commons

- cal Society of America, 111(4), 2158-2166, https://doi.org/10.1785/
- Boore, D.M. & Thompson, E.M. (2007) On using surface-source downhole-receiver logging to determine seismic slownesses. Soil Dynamics and Earthquake Engineering, 27(11), 971-985, https:// doi.org/10.1016/i.soildvn.2007.03.005.
- Borcherdt, R.D. (1994) Estimates of site-dependent response spectra for design (methodology and justification). Earthquake Spectra, 10(4), 617-653, https://doi.org/10.1193/1.1585791.
- Butcher, A.P., Campanella, R.G., Kaynia, A.M. & Massarsch, K.R. (2005) Seismic cone downhole procedure to measure shear wave velocity-a guideline prepared by ISSMGE TC10: geophysical Testing in geotechnical engineering. In: Proceedings of the XVI international conference on soil mechanics and geotechnical engineering, Osaka, Japan, 2005.
- Campanella, R.G. & Stewart, W.P. (1992) Seismic Cone Analysis Using Digital Signal Processing for Dynamic Site Characterization. Canadian Geotechnical Journal, 29(3), 477-486, https://doi.org/10.1139/
- Castellaro, S., Mulargia, F. & Rossi, P.L. (2008) Vs30: proxy for seismic amplification? Seismological Research Letters, 79(4), 540-543, https://doi.org/10.1785/gssrl.79.4.540.
- Crice, D. (2011) Near-surface, downhole shear wave surveys-a primer. The Leading Edge, 30(2), 164-171, https://doi.org/10.1190/ 1.3555327.
- D7400-19. (2019) Standard test methods for downhole seismic testing. West Conshohocken, PA: ASTM International.
- Deere, D.U. & Deere, D.W. (1988) The rock quality designation (RQD) index in practice. West Conshohocken, PA: ASTM Special Technical Publication, https://doi.org/10.1520/STP48465S
- Ghione, F., Köhler, A., Dichiarante, A.M., Aarnes, I. & Oye, V. (2023) Vs30 and depth to bedrock estimates from integrating HVSR measurements and geology-slope approach in the Oslo area, Norway. Frontiers in Earth Science, 11, 1-19, https://doi.org/10.3389/feart. 2023.1242679.
- Hallal, M.M. & Cox, B.R. (2019) Theoretical evaluation of the interval method commonly used for downhole seismic testing. In: Geocongress 2019. Reston, VA, American Society of Civil Engineers. pp. 376-386, https://doi.org/10.1061/9780784482131.038.
- Howard, J.K., Fraser, W.A. & Schultz, M.G. (2008) Probabilistic use of arias intensity in geotechnical earthquake engineering. In: Geotechnical earthquake engineering and soil dynamics IV. Reston, VA, American Society of Civil Engineers, pp. 1-10, https://doi.org/10. 1061/40975(318)6.
- Joh, S.H. & Mok, Y.J. (1998) Development of an inversion analysis technique for downhole seismic testing and continuous seismic CPT. Journal of Korea Geotechnical Society, 14(3), 95-108.
- Kalinski, M.E. (2012) A small, lightweight borehole receiver for crosshole and downhole seismic testing. Geotechnical Testing Journal, 35(2), 363-366, https://doi.org/10.1520/GTJ104156.
- Kim, D.S., Bang, E.S. & Kim, W.C. (2004) Evaluation of various downhole data reduction methods for obtaining reliable VS profiles. Geotechnical Testing Journal, 27(6), 585-597, https://doi.org/10. 1520/ati11811.
- Kim, J.H. & Park, C.B. (2002) Processing of downhole S-wave seismic survey data by considering direction of polarization. Journal of the Korean Geophysical Society, 5(4), 321-328.
- Kumar, A. & Anbazhagan, P. (2023) Integration of downhole data reduction techniques for determination of Vs profiles. In: Geocongress 2023. Reston, VA, American Society of Civil Engineers. pp. 152-161, https://doi.org/10.1061/9780784484678.005.
- Kumar, A. & Anbazhagan, P. (2025) Seismic site characterization of shallow bedrock sites in peninsular India using multiple geophysical methods. Acta Geotechnica, https://doi.org/10.1007/s11440-025-02534-w.
- Michaels, P. (2001) Use of principal component analysis to determine down-hole tool orientation and enhance SH-waves. Journal of Envi-

- ronmental and Engineering Geophysics, 6(4), 175-183, https://doi. org/10.4133/jeeg6.4.175.
- Park, C.B., Miller, R.D. & Xia, J. (1998) Imaging dispersion curves of surface waves on multi-channel record. In: SEG Technical Program Expanded Abstracts 1998, Houston, TX, Society of Exploration Geophysicists, pp. 1377–1380, https://doi.org/10.1190/1.1820161.
- Park, C.B., Miller, R.D. & Xia, J. (1999) Multichannel analysis of surface waves. Geophysics, 64(3), 800-808, https://doi.org/10.1190/1. 1444590.
- Stokoe, K.H., Hwang, S., Roberts, J.N., Meng, F.M., Keene, A.K., Lee. R.C. et al. (2017) Deep downhole seismic testing using a hydraulically-operated, controlled- waveform vibroseis, 16th World Conference on Earthquake Engineering, 16WCEE 2017, Santiago Chile, January 9th to 13th 2017 Paper No. 4582.
- Stokoe, K.H., Li, S., Cox, B., Meng, F.-Y. & Rohay, A. (2008) Deep downhole seismic testing for earthquake engineering studies. In: 14th world conference on earthquake engineering: innovation, practice, safety, 12-17, Beijing, China.
- Vergniault, C. & Mari, J.-L. (2020) 1 Shear velocity measurement in boreholes. In: Well seismic surveying and acoustic logging, Les Ulis: EDP Sciences, pp. 15-48, https://doi.org/10.1051/978-2-7598-2263-8.c003.
- Wang, H., Wu, S., Qi, X. & Chu, J. (2021a) Modified refracted ray path method for determination of shear wave velocity profiles using seismic cone. Engineering Geology, 293, 106330, https://doi.org/ 10.1016/j.enggeo.2021.106330.
- Wang, H., Wu, S., Qi, X. & Chu, J. (2021b) Site characterization of reclaimed lands based on seismic cone penetration test. Engineering Geology, 280(2), 105953, https://doi.org/10.1016/j.enggeo. 2020.105953.
- Wang, J.S., Hwang, J.H., Lu, C.C. & Deng, Y.C. (2022) Measurement uncertainty of shear wave velocity: a case study of thirteen alluvium test sites in Taipei Basin. Soil Dynamics and Earthquake Engineering, 155, 107195, https://doi.org/10.1016/j.soildyn.2022.
- Wu, W., Liu, J., Guo, L. & Deng, Z. (2020) Methodology and assessment of proxy-based Vs30 estimation in Sichuan Province, China. International Journal of Disaster Risk Science, 11(1), 133-144, https://doi.org/10.1007/s13753-020-00253-2.
- Xia, J., Miller, R.D. & Park, C.B. (1999) Estimation of near-surface shear-wave velocity by inversion of Rayleigh waves. Geophysics, 64(3), 691-700, https://doi.org/10.1190/1.1444578.

#### SUPPORTING INFORMATION

Additional supporting information can be found online in the Supporting Information section at the end of this article.

How to cite this article: Kumar, A. & Panjamani, A. (2025) Influence of subsurface refraction and wave travel path on the estimation of average V<sub>S</sub> profiles from the seismic downhole test. Near Surface Geophysics, 23, 229-251. https://doi.org/10.1002/nsg.70009

#### **APPENDIX**

onditions) on Wiley Online Library for rules of use; OA articles are governed by the applicable Creative Commons License



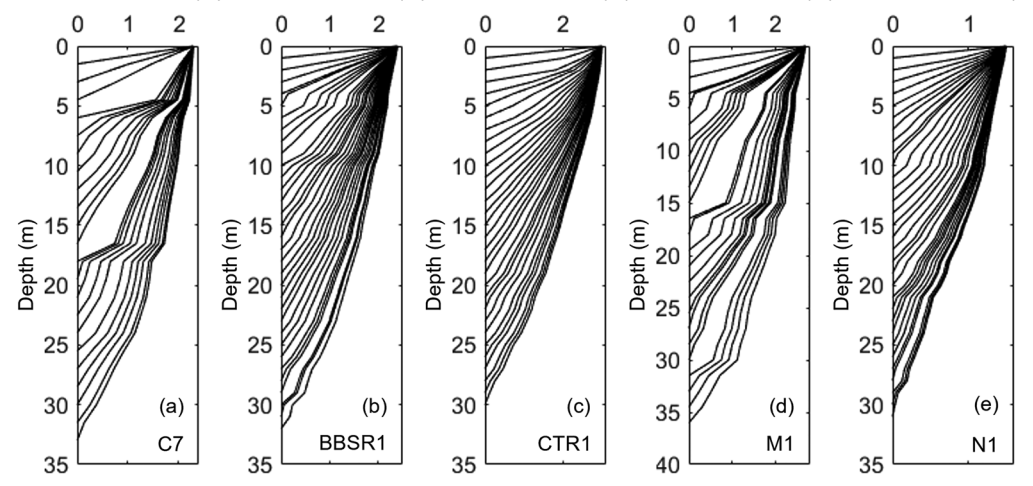


**FIGURE A1** Shows the raypaths observed for the five test locations discussed in this study. Straight raypaths are not presented to maintain clarity in figures. The error in estimate of raypath length using straight path was within 1%, in general. In shallow depths, the error was higher, 6% was observed at 6 m depth at C7 test location. Refracted raypaths for test locations (a) C7, (b) BBSR1, (c) CTR1, (d) M1 and (e) N1.

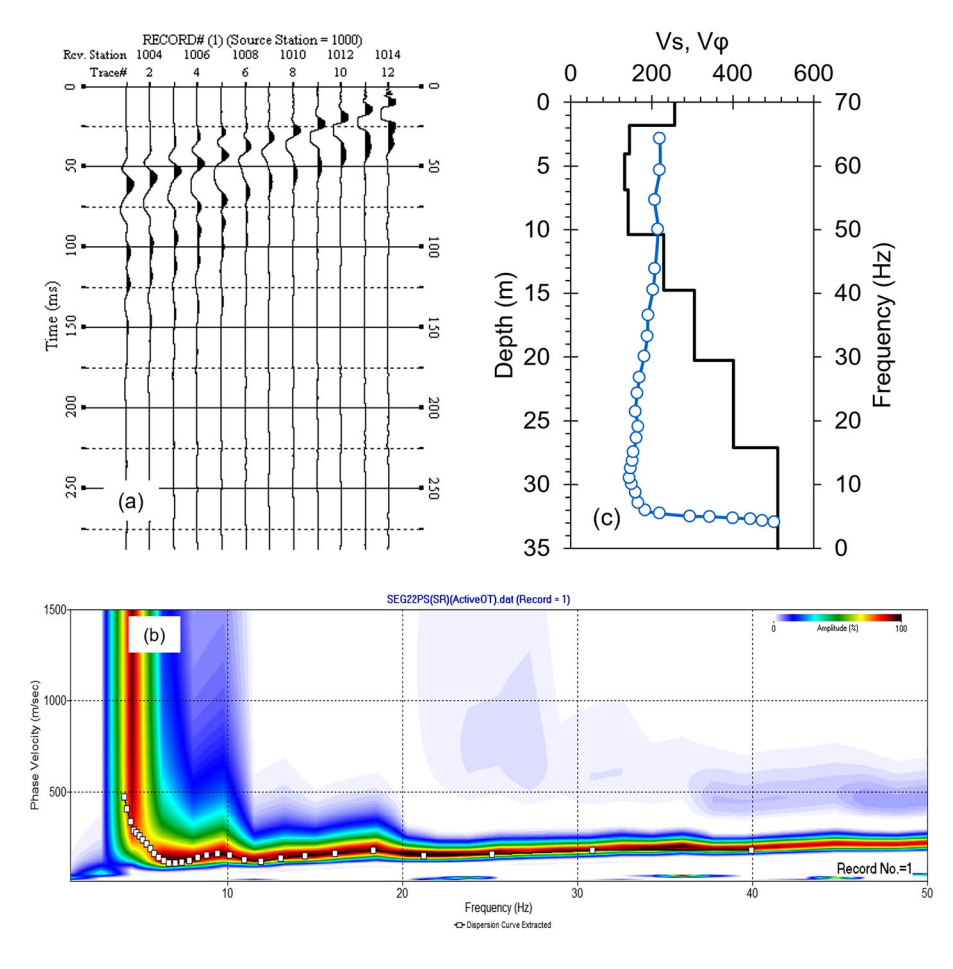


**FIGURE A2** (a) Typical waveforms acquired during MASW test, (b) dispersion image and dispersion curve and (c)  $V_S$  profile after inversion at test location C8.

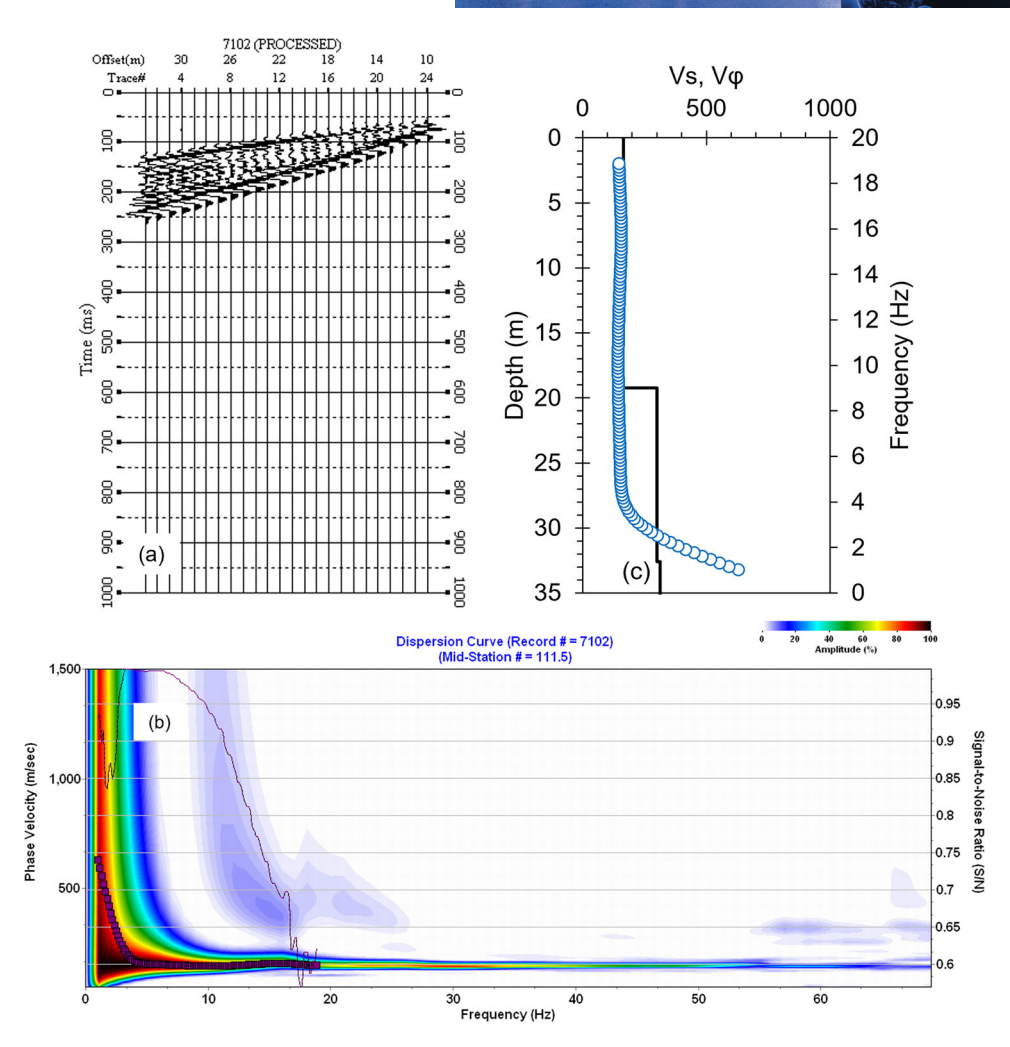


**FIGURE A3** (a) Typical waveforms acquired during MASW test, (b) dispersion image and dispersion curve and (c)  $V_S$  profile after inversion at test location BBSR1.

and-conditions) on Wiley Online Library for rules of use; OA articles are governed by the applicable Creative Commons License

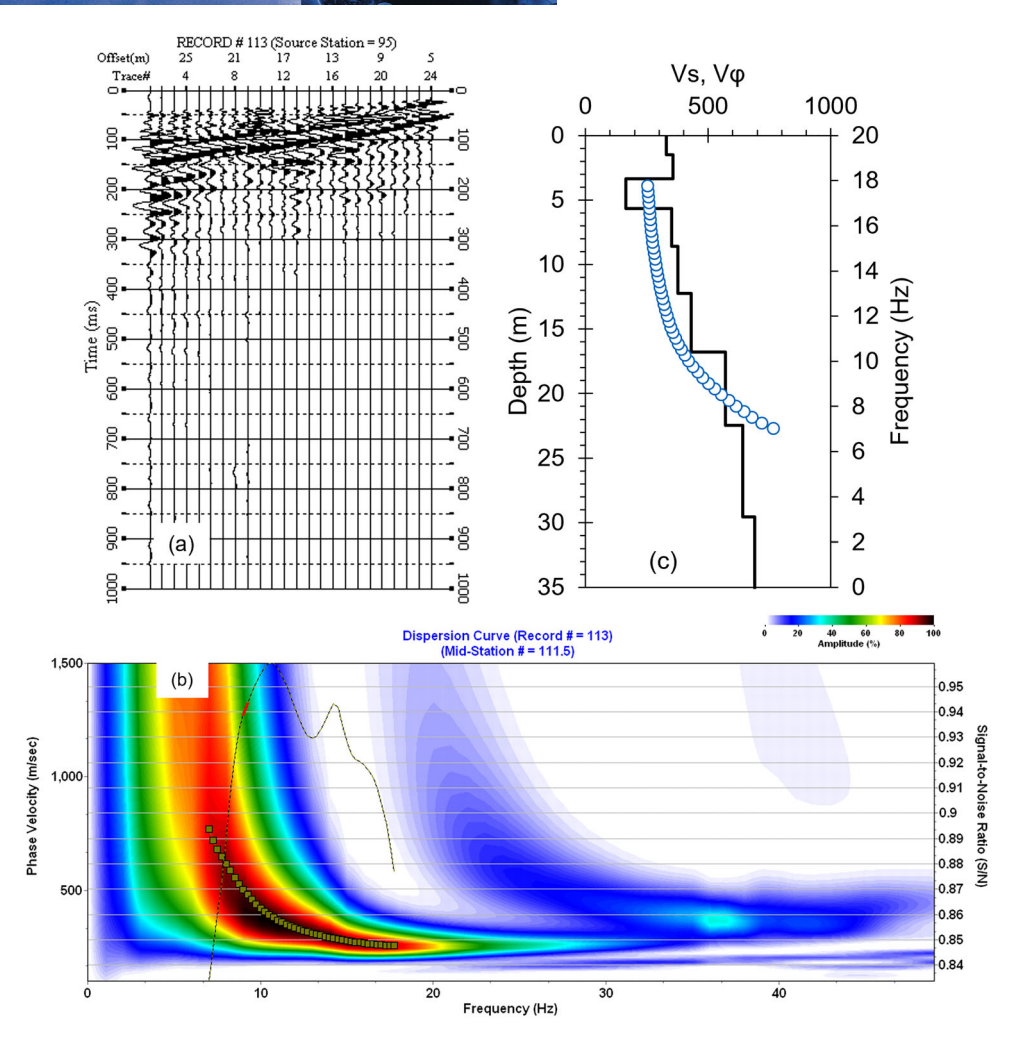


**FIGURE A4** (a) Typical waveforms acquired during MASW test, (b) dispersion image and dispersion curve and (c)  $V_S$  profile after inversion at test location CTR1.

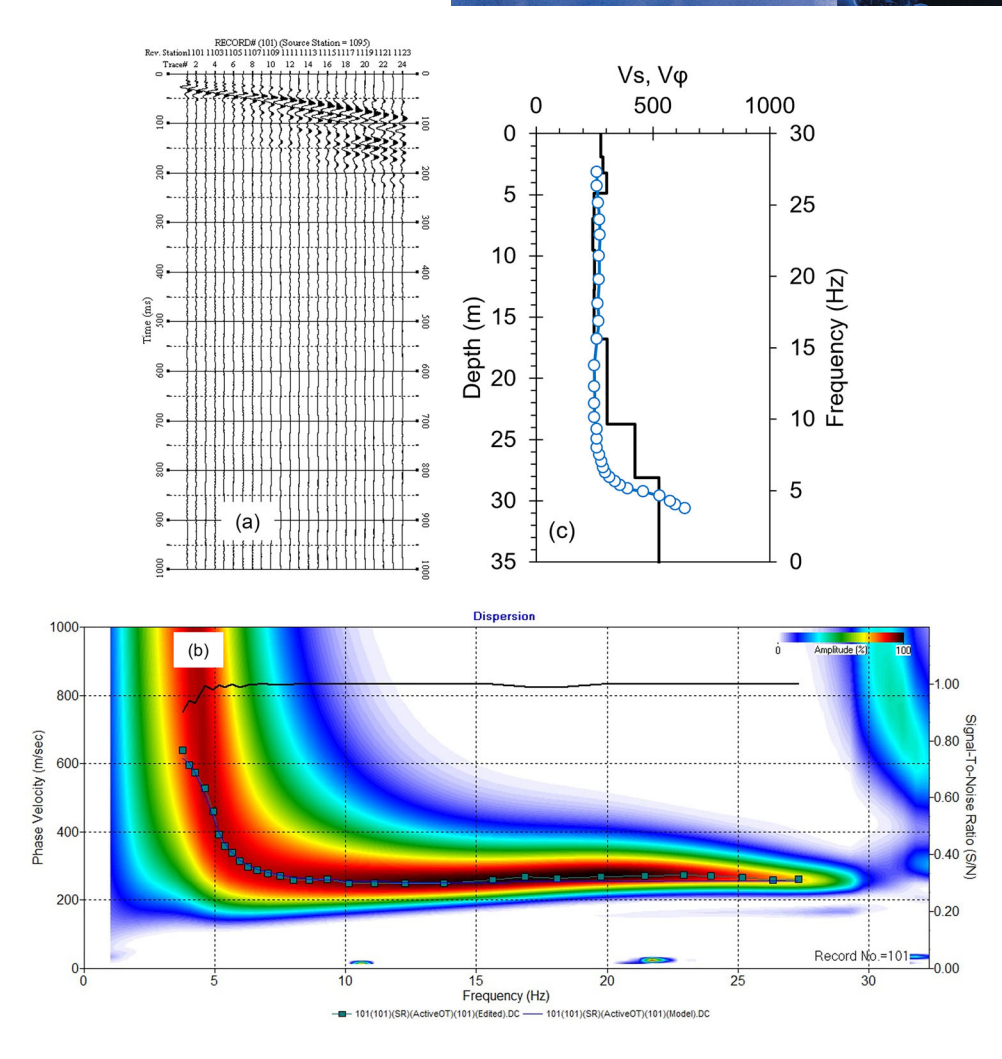


FIGURE A5 (a) Typical waveforms acquired during MASW test, (b) dispersion image and dispersion curve and (c) V<sub>S</sub> profile after inversion at test location M1.